Doctoral Dissertation

Bio-based Materials Prepared from Cellulose and Ricinoleic Acid

Bo-xing Zhang

January 2016

Graduate School of Engineering

Osaka University

Contents

Chapter 1 General introduction

Nowadays, most of products used in our everyday life come from petroleum resources. With the development of the society, the requirement for petrochemical products would further increase.[1] However, the petroleum will be depleted in an anticipated future. Furthermore, the petrochemical products are recalcitrant to the microbial attack, persisting for many years after disposal and causing serious contamination to the soil; the burning of wastes from petrochemical products releases greenhouse gas, resulting in global warming.[2,3] These realistic problems urge people to develop renewable and biodegradable materials. To meet this purpose, various types of bioresources have been explored over the last decades, such as poly(lactic acid) (PLA), polyhydroxyalkanoates (PHA), plant oil, proteins, starch, cellulose, lignin, chitin, and chitosan.[4-12]

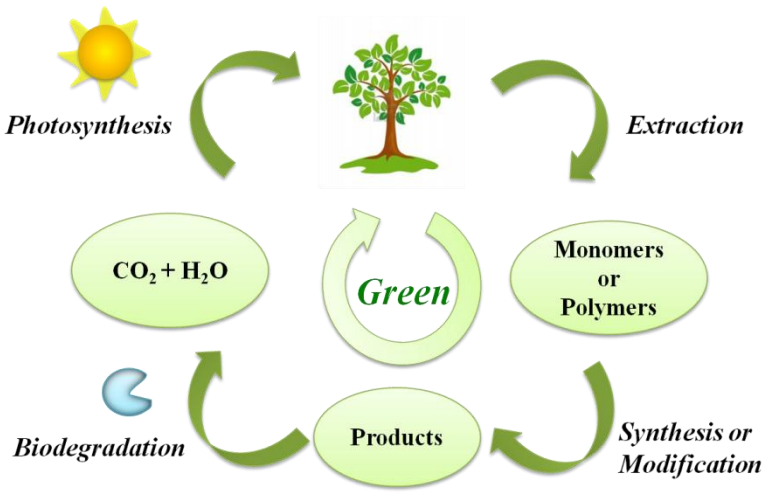

Figure 1-1. Ideal circle of biobased and biodegradable materials

In an ideal case (Figure 1-1), the biobased products are obtained from these

bioresources by synthesis or modification, and processing. After usage, the waste from these products are buried and degraded by the microbes in the soil, releasing carbon dioxide and water, which are converted to carbohydrate polymers by the photosynthesis again.[13,14] This process is totally green and sustainable. In reality, however, these biobased and biodegradable products often display poor performances, which limit their practical applications.

Plant oils and cellulose are regarded as two kinds of the most promising precursors, and receive increasing attention due to their abundant resources, extraordinary renewability, biodegradability, and unique molecular structure.[15-25]

1.1 Polymers derived from ricinoleic acid

Among different kinds of plant oils, castor oil is low cost, commercially available, and non-edible.[15,19,21] Ricinoleic acid (RA) [(9Z, 12R)-12-hydroxyoctadec-9-enoic acid] takes up of approximately 90 % of castor oil. Compared to other common fatty acid (Figure 1-2)[18], RA possesses special structure: double bond, carboxylic and hydroxyl groups coexist in the molecular structure.[26] The carboxylic and hydroxyl groups make RA polymerizable by the condensation reaction. Meanwhile, the unsaturated bonds render RA with cross-linkable properties.[27,28]

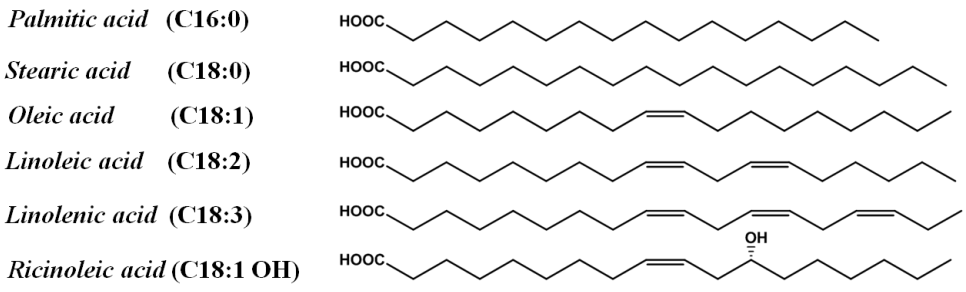

Figure 1-2. Molecular structure of common fatty acids

1.1.1 Polyesters based on RA

RA possesses poor reactivity due to the steric hindrance caused by the dangling chain. In most of previous researches, only estolides (oligomer) of RA were obtained from RA using the lipase as catalyst.[29-31] Until 2007, Ebata and Matsumura et al. synthesized a high molecular weight polyester (1.0×10^5 g/mol) from pure methyl ricinoleate using 50 wt% of immobilized lipase as catalyst, which was further cured to form a elastomer.[27,28] The obtained elastomer was strengthened with carbon black and possessed good mechanical performance with a tensile strength at break of 6.9 MPa and an elongation at break of 350 %. Although the mechanical properties were attractive, the high cost of pure methyl ricinoleate and lipase would hamper the practical applications of this elastomer.

1.1.2 Copolyesters based on RA and other monomers

To develop the materials with good performance, RA was often copolymerized with other monomers bearing rigid molecular structure. Domb and coworkers did a lot of work in this area. In 1999, Teomim and Domb et al. synthesized polyanhydrides from pure RA haft-esters with maleic and succinic anhydrides, which possessed desired physicochemical and mechanical properties for usage as drug carriers.[32] In 2003, Krasko and Domb et al. prepared new degradable poly(ester anhydride)s by the melt polycondensation of diacid oligomers of poly(sebacic acid) transesterified with RA. These polymers were degradable *in vitro* physiological conditions and could constantly release an incorporated drug for more than 2 weeks. The improved storage stability and possibility of sterilization by γ-irradiation made the polymers suitable for the

preparation of biodegradable drug-eluting devices.[33] In 2005, Krasko and Domb investigated the degradation process of poly(ricinoleic-*co*-sebacic-ester-anhydride)s in buffer solution by following the composition of the degradation products released into the degradation medium and the degraded polymers. The two-stage *in vitro* degradation process was revealed.[34] Except for sebacic acid, lactic acid (LA) was often used to copolymerize with RA. In 2005, Slivniak and Domb prepared macrolactones and polyesters from ricinoleic acid. Further, the macrolactones were copolymerized with LA by ring-opening polymerization. The results showed that the polymerization from the macrolacones only resulted in oligomers, in contrast, the copolymerization from macrolactones and LA led to relatively high molecular weights ranging from 5000 to 16000 g/mol. And, the RA-LA copolymers showed positive effects on the *in vitro* degradation rate and the physical properties due to the incorporation of RA in the polymers.[35] In 2005, Slivniak and Domb synthesized copolyester from purified RA and LA with different ratios of RA to LA by thermal polycondensation and by transesterification of high molecular weight PLA with RA and repolyesterification. The two different methods for the synthesis of copolymers of LA and RA led to random and multiblock copolymers, which showed significant differences in thermal properties even with similar composition and molecular weights.[36] In 2011, Robertson and Hillmyer synthesized poly(ricinoleic acid) (PRA)-poly(L-lactide) (PLLA) diblock copolymers, which were used to compatibilize the PLLA/castor oil blends. The tensile toughness and morphology of the blends was improved with the addition of the block copolymers.[37] In 2013, Lebarbé and Cramail et al. prepared a set of ABA triblock PLLA-*b*-PRA-*b*-PLLA copolyesters by consecutive AB type self-condensation and ring-opening polymerization. The α,ω-hydroxy-terminated PRA with molecular weight of 11 kg/mol

was synthesized from 1,3-propanediol and methyl ricinoleate, followed by polymerization with LA. The final triblock copolymers were obtained with a composition ranging from 35 to 83 wt% of PLLA, and the thermal-mechanical properties were highly dependent on the chemical composition of the block copolymers.[38] The copolymers of bile acid and RA were also reported. In 2008, Gautrot and Zhu synthesized high molecular weight copolyesters from bile acid and RA by entropy-driven ring-opening metathesis polymerizations, and the copolyesters displayed tunable mechanical properties and degradation behaviors.[39] In the above researches, although the copolymers with good performance were successfully synthesized, RA was commonly used as a minor component to tune the properties of the copolymers.

1.1.3 Hyperbranched polymers based on RA

In recent years, hyperbranched polymers have received much attention due to their multiple functional groups, low viscosity, good film-forming properties, and easy crosslinking properties.[40-42] Instead of linear types of polymers, hyperbranched polymers were also prepared from RA in the previous researches. In 2006, Kelly and Hayes prepared tetra-branched PRA with average molecular weight of 4850 g/mol from pentaerythritol and RA using the immobilized lipase as catalyst.[43] Karak and coworkers also did some work in this area. In 2009, Karak and Cho et al. synthesized a series of castor oil-modified hyperbranched polyurethane *via* $A_2 + B_3$ approach. Except for castor oil, macroglycol poly(ε-caprolactone)diol or poly(ethylene glycol), and diphenyl methane diisocynate were used.[44] In 2013, Pramanik and Karak et al. synthesized hyperbranched polyesteramide using *N,N'*-bis(2-hydroxyethyl) castor oil fatty amide, phthalic anhydride, maleic anhydride, and isophthalic acid as A_2 monomers, and

diethanol amine as B_3 monomer. The obtained hyperbranched polymers could be used advanced biodegradable surface coating materials.[45,46] In 2014, De and Karak et al. synthesized a tough, elastic, biodegradable, and thermostable hyperbranched epoxy from castor oil based polyol, bis(hydroxyl methyl)propionic acid, and diglycidal ether of bisphenol A.[47] A hyperbranched polymer was also synthesized from dipentaerythritol, dimethylopropionic acid, and ricinoleic acid, and used for tamoxifen and idarubicin delivery.[48] There were a large portion of petroleum-based resources employed to construct the previous hyperbranched polymers, which will inevitably compromise the green concept.

Although a variety of materials based on RA have been synthesized, it was found that either the content of RA was low, or no good mechanical performance was achieved with high content of RA. Herein, further researches need to be done to improve the mechanical performance of the materials with RA as the main component.

1.2 Applications of cellulose

Cellulose is the most abundant renewable and biodegradable polymer in the world. It is composed of polydispersed linear poly-β(1,4)-D-glucose molecules with syndiotactic configuration (Fig. 1-3).[49] There are six polymorphs of crystalline cellulose (I, II, III_I, III_{II}, IV_I, and IV_{II}), which could be interconverted.[50] Cellulose I is naturally produced by plants and bacteria, sometimes referred to as natural cellulose, and can be further divided to triclinic I_α and monoclinic I_β polymorphs: the former mainly comes from algae and bacteria; the latter chiefly derives from higher plants.[22,24,51] Cellulose powder could be extracted from a wide range of plants, such as wood, hemp, cotton, and linen for material applications, and further processed to cellulose microfibrils and

cellulose nanocrystals.[23,24,52] With the development of the technology, the applications of cellulose have not been limited to forest products, paper, textiles, etc, which have been used for thousands of years in human society. Advanced materials based on cellulose have been developed in recent years, such as cellulose film, hydrogel, aerogel, and composites. Because this thesis mainly deals with the fabrication of cellulose film and composites, the researches related to cellulose film and composites would be introduced in the following content.

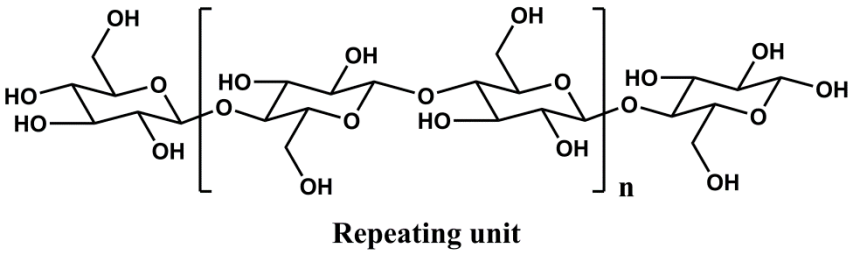

Figure 1-3. Molecular structure of cellulose

1.2.1 Cellulose solvent

Cellulose cannot melt under heating or dissolve in aqueous and orgainc solvents, due to strong hydrogen bonds exiting in the molecular structure.[53] Dissolution of cellulose is an indispensable prerequisite for processing and fabricating cellulose products. The viscose process, invented by Cross and co-workers in 1982, is the first and most important route to cellulose solutions, and still practiced today with an output of about 3 million tons annually worldwide.[54] The Cuam process, using aqueous solutions of cuproethylene diamine or cuprammonium hydroxide as cellulose solvent, is also well known for a rather long time and still maintains its importance for production of staple fibres, filaments, membranes, and the determination of the molecular weight of cellulose by viscometry.[54] In recent decades, several different kinds of cellulose solvents

have been developed, which could be categorized to two main types of derivatizing and non-derivatizing solvents, and further classified to aqueous and non-aqueous solvents. The term "non-derivatizing" denotes that the solvents dissolve the cellulose by intermolecular interactions only, while the group of "derivatizing" solvents dissolves cellulose by forming ether, ester, or acetal derivatives with cellulose. Among these solvents, urea and sodium hydroxide solution and *N*-methylmorpholine-*N*-oxide (NMMO) monohydrate are famous for the applications in CarbaCell process and Lyocell process, which have been applied in industrial field.[22] Besides, LiCl/*N*,*N*-dimethylacetamide (DMAc) solvent also has important applications for the analysis of cellulose structure and preparation of a wide variety of derivatives of cellulose due to the negligible degradation of cellulose during the dissolution and storage process.[54-56]

1.2.2 Cellulose films

Cellophane is the first reported cellulose film fabricated from the Viscose route, and nowadays still has important applications for food casing. Cuprophane is another old material prepared from Cuam process, and keeps important applications for dialysis.[57] In recent years, the usage of Viscose and Cuam processes were suppressed due to the increasing environment concerning.[22,54] Instead, less harmful CarbaCell and Lyocell processes were employed with an increasing trend.[22,53,57-62] In 2007, Gindl and Keckes fabricated self-reinforced cellulose film by incomplete dissolution of microcrystalline cellulose in LiCl/DMAc solvent, subsequent regeneration, drawing in the wet state, and drying process.[63] Except for these regeneration methods, other methods were also used to prepared cellulose film, such as the stacking of cellulose

nanofiber. In 2009, Nogi and Yano et al. fabricated a transparent film from nanofiber by the suspension of the nanofiber in water, slow filtration, drying, and polishing process. The obtained film possessed good transparency (72 % at a wavelength of 600 nm), high strength (223 MPa), high modulus (13 GPa), and minimal thermal expansion (8.5 ppm/k).[64] In the same year, Fukuzumi and Isogai et al. prepared transparent cellulose films from cellulose nanofiber by 2,2,6,6-tetramethylpiperidine-1-oxyl radical (TEMPO)-mediated oxidation. The final film possessed high oxygen barrier properties and extremely low coefficient of thermal expansion (2.7 ppm/k) caused by high crystallinity of native cellulose.[65] Most of cellulose films prepared from regeneration method possessed cellulose II structure,[22] while the cellulose films from nanofiber may remain the cellulose I structure of the original cellulose, and no amorphous cellulose films were reported.

1.2.3 Composites based on cellulose

A lot of researches focus on the applications of cellulose in composite materials, due to low density, high strength and stiffness of cellulose.[23,52,66,67] Solution blending is one kind of methods for fabricating cellulose composites, and Nishio and Manley et al. did some pioneering work in this area. Between 1987 and 1990, Nishio and Manley et al. sequentially blended cellulose with polyacrylonitrile, poly(vinyl alcohol) (PVA), nylon 6, and poly(ε-caprolactone) from LiCl/DMAc solution by coagulation in a non-solvent.[68-70] In 1991, Masson and Manley prepared blend films of cellulose and poly(vinylpyrrolidone) from the mixing solution of cellulose solution in dimethyl sulfoxide-paraformaldehyde and poly(vinylpyrrolidone) solution in DMSO by slow casting under reduced pressure.[71] The binary components in all of these blend films

showed good miscibility. In 2011, Kim and Park et al. prepared graphene oxide (GO) and cellulose composite films from NMMO solution by coagulation. The introduction of GO to the cellulose matrix made the composite film strong but brittle.[72] In 2012, similarly, Zhang and Zhu et al. prepared GO and cellulose composite films from LiCl/DMAc solution by coagulation. The results showed that GO was nano-dispersed in cellulose matrix, and the thermal-mechanical properties and the electrical conductivity were improved.[73] In 2012, Zhang and Zhu et al. prepared the thermoplastic polyurethane (TPU) elastomer and cellulose composite films, which displayed improved toughness and oxygen barrier properties with the addition of TPU.[74] In 2012, Zhang and Zhu et al. also prepared PVA and cellulose composite films from ionic liquid 1-ally-3-methylimidazolium chloride (AMIMCl) solution by coagulation. The composite films demonstrated improved mechanical properties and shrinkage compared to cellulose films.[75] In 2011, Morgado and Coma prepared chitosan and cellulose blend films from NaOH/thiourea solution. The increase of chitosan in the composite films could promote the tensile strength and elongation at break.[76] The abovementioned composite films share common features that all of them were prepared from solution blending and regeneration method, and good miscibility between the binary components could be achieved. However, this method is only applicable for the polar components that could be dissolved in cellulose solvents.

As for composites of cellulose and non-polar components, the impregnation method was often used. In 2000, Williams and Wool successfully prepared composites from natural fiber and soybean oil resins by resin transfer molding process (RTM). The composites showed good mechanical performance with tensile strength of 30 MPa, tensile modulus of 5 GPa.[77] In 2004, O'Donnell and Wool et al. made composites panels

out of acrylated epoxidized soybean oil (AESO) and natural fiber mats of flax, cellulose powder, pulp, and hemp by vacuum-assisted resin transfer molding or resin vacuum infusion process. The flexural modulus of the final composites with 10-50 wt% of natural fiber was increased to a range between 1.5 to 6 GPa depending on the nature of fiber mats.[78] In the above researches, although the mechanical properties of composites were largely improved, the inhomogeneous distributions of natural fiber still need to be dissolved. In our lab, a cellulose hydrogel with uniform porous structure was prepared from $Ca(SCN)_2$ aqueous solution by regeneration and washing. Subsequently the cellulose and Poly(3-hydroxybutyrate-co-3-hydroxyhexanoate) (PHBH) composite film was obtained by immersing the hydrogel into PHBH solution, followed by drying and hot pressing. The composite films showed good transparency and improved mechanical properties compared to PHBH.[79] Except for the cellulose gel regenerated from cellulose solution, bacterials cellulose also possesses homogenous porous structure and can be used to strengthen resin matrix. In 2008, Nogi and Yano prepared highly transparent composite films from bacterial cellulose and acrylic resin by the impregnation method. The composite films possessed ultra low coefficient of thermal expansion, good flexibility, and thermal stability.[80] In 2012, Retegi and Mondragon et al. obtained transparent composite films from bacterial cellulose and epoxidized soybean oil (ESO) using a similar method with that of Nogi and Yano. It can be known that the composite films with good optical and mechanical performance have been obtained by the impregnation method. However, the complexity of impregnation method would inevitably increase the cost and requirements for the instruments, and eventually limit the wide applications. Alternative methods still need to be explored.

1.3 Composition and functions of plant cuticle

Plant cuticle covers nearly all aerial parts of terrestrial plants and forms the interface between plant and environment with the thickness varying widely among different plant species and different organs of the same plant (0.02 ~ 200 μm).[81] It is mainly composed of epicuticular and intracuticular waxes, cutin, polysaccharides, glycerol, and small amounts of phenolics. Cutin is a matrix of polyhydroxylated C_{16} and/or C_{18} fatty acids cross-linked by ester bonds. The waxes deposit on the surface of cutin (epicuticular waxes) or embed in the cutin matrix (intracuticular waxes). The polysaccharides including cellulose, hemicellulose, and pectin mix with cutin and meanwhile connect to the outer epidermal cell walls (Fig. 1-4).[82,83] The whole cuticle functions as a biological barrier to regulate gas exchange and protect the plants from water loss, mechanical injury, pathogen attack, and UV damage.[84]

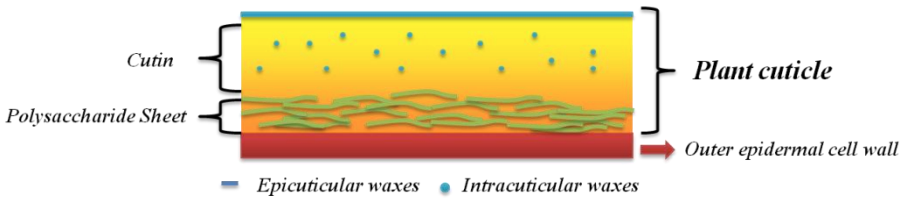

Figure 1-4. Schematic structure of plant cuticle

From the perspective of materials science, the plant cuticle is an ideal bio-based packaging material with well-balanced performance. However, such materials could not be extracted from plants for practical applications due to the difficulty of extraction and processing, which encourages the biomimicry of plant cuticle. In 2004, Benítez and Heredia et al. synthesized an aliphatic polyester identical to natural cutin using the monomers extracted from tomato for the first time.[85] In 2009, Heredia-Guerrero and Benítez et al. prepared a mimetic polymer of plant cutin from

9,10,16-trihydroxyhexadecanoic (aleuritic) acid through the polycondensation reaction.[86] Although the plant cutin was successfully mimicked, there is still a long way to run until the practical application. Besides, the mimicry of plant cuticle was rarely reported.

1.4 Purpose and outline of this thesis

This thesis focuses on the preparation of biobased materials from RA and cellulose towards practical applications. First, the biobased materials were prepared separately from RA and cellulose, then the double layer composites of them was fabricated enlightened by plant cuticle. The good performance of the composites was expected to achieve by combination of the advantages of the RA and cellulose. This thesis consists of six chapters including general introduction (chapter 1) and concluding remarks (chapter 6).

In chapter 2, a highly transparent cellulose film was fabricated from cellulose powder (cotton resource) by regeneration from the LiCl/DMAc solution. The structure and properties of cellulose film were investigated with various techniques.

In chapter 3, linear polyricinoleic acid (LPRA) and tri-branched polyricinoleic acid (BPRA) were synthesized using immobilized lipase as catalyst, and were further incorporated separately into the matrix of *trans*-1,4-polyisoprene extracted from *Eucommia ulmoides* Oliver (EuTPI) as processing aid. The morphology, crystallization behaviors, thermal stability, mechanical and rheological properties of the blend films were systematically investigated.

In chapter 4, a hyperbranched poly(ricinoleic acid) (HBPRA) was prepared based on polyglycerol (PGL) and RA with *p*-toulenesulfonic acid (PTSA) as catalyst.

The reaction conditions, structure, and properties of HBPRA were extensively studied.

In chapter 5, a biomimic plant cuticle was successfully fabricated from HBPRA and cellulose film with the aid of UV-initiated thio-ene click reaction. The transparency, morphology, surface properties, and mechanical properties of biomimic cuticle were systematically investigated.

1.5 References

(1) Mülhaupt, R. *Macromol. Chem. Phys.* **2013,** *214*, 159-174.

(2) Khoo, H.; Tan, R. H. *Int. J. Life Cycle Assess* **2010,** *15*, 338-345.

(3) Sudesh, K.; Iwata, T. *Clean* **2008,** *36*, 433-442.

(4) Reddy, M. M.; Vivekanandhan, S.; Misra, M.; Bhatia, S. K.; Mohanty, A. K. *Prog. Polym. Sci.* **2013,** *38*, 1653-1689.

(5) Mekonnen, T.; Mussone, P.; Khalil, H.; Bressler, D. *J. Mater. Chem. A* **2013,** *1*, 13379-13398.

(6) Babu, R.; O'Connor, K.; Seeram, R. *Prog. Biomater.* **2013,** *2*, 1-16.

(7) Satyanarayana, K. G.; Arizaga, G. G. C.; Wypych, F. *Prog. Polym. Sci.* **2009,** *34*, 982-1021.

(8) DiGregorio, B. E. *Chem. Biol.* **2009,** *16*, 1-2.

(9) Chen, G.-Q. *Chem. Soc. Rev.* **2009,** *38*, 2434-2446.

(10) Dale, B. E. *J. Chem. Technol. Biotechnol.* **2003,** *78*, 1093-1103.

(11) Mohanty, A. K.; Misra, M.; Drzal, L. T. *J. Polym. Environ.* **2002,** *10*, 19-26.

(12) Chiellini, E.; Solaro, R. *Adv. Mater.* **1996,** *8*, 305-313.

(13) Gross, R. A.; Kalra, B. *Science* **2002,** *297*, 803-807.

(14) Tharanathan, R. N. *Trends Food Sci. Technol.* **2003,** *14*, 71-78.

(15) Kunduru, K. R.; Basu, A.; Haim Zada, M.; Domb, A. J. *Biomacromolecules* **2015,** *16*, 2572-2587.

(16) Miao, S.; Wang, P.; Su, Z.; Zhang, S. *Acta Biomater.* **2014,** *10*, 1692-1704.

(17) Islam, M. R.; Beg, M. D. H.; Jamari, S. S. *J. Appl. Polym. Sci.* **2014,** *131*, 1-13

(18) Biermann, U.; Bornscheuer, U.; Meier, M. A. R.; Metzger, J. O.; Schäfer, H. J. *Angew. Chem. Int. Ed.* **2011,** *50*, 3854-3871.

(19) Mutlu, H.; Meier, M. A. R. *Eur. J. Lipid Sci. Technol.* **2010,** *112*, 10-30.

(20) Seniha Güner, F.; Yağcı, Y.; Tuncer Erciyes, A. *Prog. Polym. Sci.* **2006,** *31*, 633-670.

(21) Ogunniyi, D. S. *Bioresour. Technol.* **2006,** *97*, 1086-1091.

(22) Klemm, D.; Heublein, B.; Fink, H.-P.; Bohn, A. *Angew. Chem. Int. Ed.* **2005,** *44*, 3358-3393.

(23) Kalia, S.; Dufresne, A.; Cherian, B. M.; Kaith, B. S.; Avérous, L.; Njuguna, J.; Nassiopoulos, E. *Int. J. Polym. Sci.* **2011,** *2011*, 1-35.

(24) Moon, R. J.; Martini, A.; Nairn, J.; Simonsen, J.; Youngblood, J. *Chem. Soc. Rev.* **2011,** *40*, 3941-3994.

(25) Metzger, J. O.; Bornscheuer, U. *Appl. Microbiol. Biotechnol.* **2006,** *71*, 13-22.

(26) Lligadas, G.; Ronda, J. C.; Galià, M.; Cádiz, V. *Mater. Today* **2013,** *16*, 337-343.

(27) Ebata, H.; Yasuda, M.; Toshima, K.; Matsumura, S. *J. Oleo Sci.* **2008,** *57*, 315-320.

(28) Ebata, H.; Toshima, K.; Matsumura, S. *Macromol. Biosci.* **2007,** *7*, 798-803.

(29) Yoshida, Y.; Kawase, M.; Yamaguchi, C.; Yamane, T. *J. Am. Oil Chem. Soc.* **1997,** *74*, 261-267.

(30) Bódalo-Santoyo, A.; Bastida-Rodríguez, J.; Máximo-Martín, M. F.; Montiel-Morte, M. C.; Murcia-Almagro, M. D. *Biochem. Eng. J.* **2005,** *26*, 155-158.

(31) Bódalo, A.; Bastida, J.; Máximo, M. F.; Montiel, M. C.; Gómez, M.; Murcia, M. D. *Biochem. Eng. J.* **2008,** *39*, 450-456.

(32) Teomim, D.; Nyska, A.; Domb, A. J. *J. Biomed. Mater. Res.* **1999,** *45*, 258-267.

(33) Krasko, M. Y.; Shikanov, A.; Ezra, A.; Domb, A. J. *J. Polym. Sci. Part A: Polym. Chem.* **2003,** *41*, 1059-1069.

(34) Krasko, M. Y.; Domb, A. J. *Biomacromolecules* **2005,** *6*, 1877-1884.

(35) Slivniak, R.; Domb, A. J. *Biomacromolecules* **2005,** *6*, 1679-1688.

(36) Slivniak, R.; Langer, R.; Domb, A. J. *Macromolecules* **2005,** *38*, 5634-5639.

(37) Robertson, M. L.; Paxton, J. M.; Hillmyer, M. A. *ACS Appl. Mater. Interfaces* **2011,** *3*, 3402-3410.

(38) Lebarbe, T.; Ibarboure, E.; Gadenne, B.; Alfos, C.; Cramail, H. *Polym. Chem.* **2013,** *4*, 3357-3369.

(39) Gautrot, J. E.; Zhu, X. X. *Chem. Commun.* **2008,** *0*, 1674-1676.

(40) Johansson, K.; Bergman, T.; Johansson, M. *ACS Appl. Mater. Interfaces* **2009,** *1*, 211-217.

(41) Gao, C.; Yan, D. *Prog. Polym. Sci.* **2004,** *29*, 183-275.

(42) Yates, C. R.; Hayes, W. *Eur. Polym. J.* **2004,** *40*, 1257-1281.

(43) Kelly, A. R.; Hayes, D. G. *J. Appl. Polym. Sci.* **2006,** *101*, 1646-1656.

(44) Karak, N.; Rana, S.; Cho, J. W. *J. Appl. Polym. Sci.* **2009,** *112*, 736-743.

(45) Pramanik, S.; Konwarh, R.; Sagar, K.; Konwar, B. K.; Karak, N. *Prog. Org. Coat.* **2013,** *76*, 689-697.

(46) Pramanik, S.; Hazarika, J.; Kumar, A.; Karak, N. *Ind. Eng. Chem. Res.* **2013,** *52*, 5700-5707.

(47) De, B.; Gupta, K.; Mandal, M.; Karak, N. *ACS Sustain. Chem. Eng.* **2014,** *2*, 445-453.

(48) Ortega, S.; Máximo, M. F.; Montiel, M. C.; Murcia, M. D.; Arnold, G.; Bastida, J. *Bioprocess Biosyst. Eng.* **2013,** *36*, 1291-1302.

(49) Hon, D. S. *Cellulose* **1994,** *1*, 1-25.

(50) Osullivan, A. C. *Cellulose* **1997,** *4*, 173-207.

(51) Habibi, Y.; Lucia, L. A.; Rojas, O. J. *Chem. Rev.* **2010,** *110*, 3479-3500.

(52) Siró, I.; Plackett, D. *Cellulose* **2010,** *17*, 459-494.

(53) Zhang, L. N.; Ruan, D.; Zhou, J. P. *Ind. Eng. Chem. Res.* **2001,** *40*, 5923-5928.

(54) Heinze, T.; Koschella, A. *Polímeros* **2005,** *15*, 84-90.

(55) Dawsey, T. R.; McCormick, C. L. *J. Macromol. Sci. Part C: Polym. Rev.* **1990,** *30*, 405-440.

(56) McCormick, C. L.; Callais, P. A.; Hutchinson, B. H. *Macromolecules* **1985,** *18*, 2394-2401.

(57) Fink, H. P.; Weigel, P.; Purz, H. J.; Ganster, J. *Prog. Polym. Sci.* **2001,** *26*, 1473-1524.

(58) Geng, H.; Yuan, Z.; Fan, Q.; Dai, X.; Zhao, Y.; Wang, Z.; Qin, M. *Carbohydr. Polym.* **2014,** *102*, 438-444.

(59) Yang, Q.; Fukuzumi, H.; Saito, T.; Isogai, A.; Zhang, L. *Biomacromolecules* **2011,** *12*, 2766-2771.

(60) Yang, Q.; Qin, X.; Zhang, L. *Cellulose* **2011,** *18*, 681-688.

(61) Yang, Q.; Saito, T.; Isogai, A. *Cellulose* **2012,** *19*, 1913-1921.

(62) Qi, H.; Chang, C.; Zhang, L. *Green Chem.* **2009,** *11*, 177-184.

(63) Gindl, W.; Keckes, J. *J. Appl. Polym. Sci.* **2007,** *103*, 2703-2708.

(64) Nogi, M.; Iwamoto, S.; Nakagaito, A. N.; Yano, H. *Adv. Mater.* **2009,** *21*, 1595-1598.

(65) Fukuzumi, H.; Saito, T.; Wata, T.; Kumamoto, Y.; Isogai, A. *Biomacromolecules* **2009,** *10*, 162-165.

(66) Azizi Samir, M. A. S.; Alloin, F.; Dufresne, A. *Biomacromolecules* **2005,** *6*, 612-626.

(67) Bledzki, A. K.; Gassan, J. *Prog. Polym. Sci.* **1999,** *24*, 221-274.

(68) Nishio, Y.; Manley, R. S. *Polym. Eng. Sci.* **1990,** *30*, 71-82.

(69) Nishio, Y.; Manley, R. S. J. *Macromolecules* **1988,** *21*, 1270-1277.

(70) Nishio, Y.; Roy, S. K.; Manley, R. S. *Polymer* **1987,** *28*, 1385-1390.

(71) Masson, J. F.; Manley, R. S. *Macromolecules* **1991,** *24*, 6670-6679.

(72) Kim, C.-J.; Khan, W.; Kim, D.-H.; Cho, K.-S.; Park, S.-Y. *Carbohydr. Polym.* **2011,** *86*, 903-909.

(73) Zhang, X.; Liu, X.; Zheng, W.; Zhu, J. *Carbohydr. Polym.* **2012,** *88*, 26-30.

(74) Zhang, X.; Zhu, J.; Liu, X.; Feng, J. *Cellulose* **2012,** *19*, 121-126.

(75) Zhang, X.; Zhu, J.; Liu, X. *Macromol. Res.* **2012,** *20*, 703-708.

(76) Morgado, D. L.; Frollini, E.; Castellan, A.; Rosa, D. S.; Coma, V. *Cellulose* **2011,** *18*, 699-712.

(77) Williams, G.; Wool, R. *Appl. Compos. Mater.* **2000,** *7*, 421-432.

(78) O'Donnell, A.; Dweib, M. A.; Wool, R. P. *Compos. Sci. Technol.* **2004,** *64*, 1135-1145.

(79) Hosoda, N.; Tsujimoto, T.; Uyama, H. *ACS Sustain. Chem. Eng.* **2014,** *2*, 248-253.

(80) Nogi, M.; Yano, H. *Adv. Mater.* **2008,** *20*, 1849-1852.

(81) Nawrath, C. *Curr. Opin. Plant Biol.* **2006,** *9*, 281-287.

(82) Dominguez, E.; Heredia-Guerrero, J. A.; Heredia, A. *New Phytol.* **2011,** *189*, 938-949.

(83) Buda, G. J.; Isaacson, T.; Matas, A. J.; Paolillo, D. J.; Rose, J. K. C. *Plant J.* **2009,** *60*, 378-385.

(84) Dominguez, E.; Cuartero, J.; Heredia, A. *Plant Sci.* **2011,** *181*, 77-84.

(85) Beniitez, J. J.; Garcia-Segura, R.; Heredia, A. *BBA-Gen. Subjects* **2004,** *1674*, 1-3.

(86) Heredia-Guerrero, J. A.; Heredia, A.; Garcia-Segura, R.; Benitez, J. J. *Polymer* **2009,** *50*, 5633-5637.

Chapter 2 Preparation and characterization of a transparent amorphous cellulose film

2.1 Introduction

The molecular chains in amorphous cellulose are loosely arranged, unlike their tight compaction in cellulose's crystalline counterpart, which should cause a significant difference in some aspects, such as in its mechanical properties,[1] reaction kinetics,[2] and enzymatic hydrolysis rate.[3-5] Some special applications, such as enzyme screening and displaying material, could be developed using amorphous cellulose film (ACF). Meanwhile, it is of great importance to investigate the behaviors of ACF for better utilization of this cellulose resource. However, most cellulose films reported to date possess the crystalline structure with cellulose II, since it is thermodynamically more stable than the other allomorphs.[6-8] In contrast, ACF with a good performance has rarely been reported, even though many methods have been developed to prepare amorphous cellulose samples, such as ball milling,[9] hydrolysis of cellulose triacetate,[10] regeneration from cadmium ethylenediamine,[11] sodium cellulose xanthates,[12] cuprammonium hydroxide,[16] dimethylsulfoxide/paraformaldehyde,[13] phosphoric acid,[13] and from SO_2/diethylamine/dimethylsulfoxide solution.[14] Moreover, most of these methods either used toxic reagents or inevitably caused degradation of the cellulose, which were the major disadvantages for scientific studies and for the practical application of ACF.

The cellulose solvent of LiCl-*N*,*N*-dimethylacetamide (DMAc) was first reported by McCormick and Lichatowich in 1979.[15] Initially, water swelled and opened the structure, and the intermolecular and intramolecular hydrogen bonds were replaced

by hydrogen links with H_2O. Then, methanol and DMAc were introduced subsequently to remove water and to impede the re-formation of the intermolecular and intramolecular hydrogen bonds. In the final step, the swollen sample was added into LiCl-DMAc solvent, with stirring until dissolved.[16,17] Although the mechanism of dissolution remained controversial, one generally accepted principle was that $[DMAc_n + Li]^+$ macrocation evolved, leaving the chloride anion (Cl^-) free. Thereby, Cl^-, being highly active as a nucleophilic base, was able to play a major role by breaking up the intermolecular and intramolecular hydrogen bonds.[15-20] The whole process was operated under mild conditions, and no appreciable degradation occurred. In addition, the cellulose solution in LiCl-DMAc was reported to be extremely stable,[16,17] which made it attractive for practical application. However, only a few reports were related to the preparation of cellulose film from LiCl-DMAc solution.[21-28] Moreover, none of them mentioned the fabrication of ACF.

In this chapter, ACF with excellent transparency was prepared by regeneration from LiCl-DMAc solution. The relationships between the concentration of cellulose solution and the mechanical properties were systematically investigated. We also compared the enzymatic hydrolysis rate of ACF and commercially available cellophane. This chapter aims to provide a simple, less-destructive, and universal method to prepare amorphous cellulose film, and, in addition, to enhance our understanding about the behaviors of amorphous cellulose to open it up to new practical applications.

2.2 Experimental section

2.2.1 Materials

Whatman CF11 fibrous medium cellulose powder (CF11, cotton origin, 50-350

μm, GE Healthcare Life Science Corp., Piscataway, NJ, USA), microcrystalline cellulose powder (Merck, cotton origin, 20-160 μm, ≥80%, Merck KGaA, Darmstadt, Germany), Avicel SF microcrystalline cellulose powder for thin layer chromatography (Avicel, pulp origin, mean particle size around 10 μm, Funakoshi, Co. Ltd., Tokyo, Japan), and bacterial cellulose prepared as described previously, except for under static condition (BC, *Gluconacetobacter xylinus* (Brown) Yamada *et al.* ATCC 53524),[29] were used as the cellulose resource. For reference, an amorphous cellulose sample derived from CF11 was prepared by a vibrating ball-mill in a N_2 atmosphere for 48 h by using ceramic balls (Ball-mill, Type MB-1 Vibrating mill, Chuo Kakohki, Co. Ltd., Nagoya, Japan).[9] Cellophane (thickness ≈ 22 μm) without any additives and coating was supplied by Futamura Chemical Co. Ltd., Nagoya, Japan. *N*,*N*-Dimethylacetamide (DMAc, purity > 99%) was obtained from Tokyo Chemical Industry Co. Ltd., Japan. Anhydrous lithium chloride (LiCl), D-glucose, anhydrous citric acid, 3,5-dinitrosalicylic acid (DNS), potassium sodium L-(+)-tartrate tetrahydrate (Rochelle salt), methanol, and acetone were obtained from Wako Pure Chemical Industries Ltd., Japan. Cellulase from *Aspergillus niger* (activity ≥ 60 000 units per mg) was obtained from MP Biomedicals, LLC., Santa Ana, CA, USA. All other reagents not specially mentioned were used as received.

2.2.2 Preparation of cellulose solution

The first step was the fabrication of cellulose solution from different cellulose resources. To facilitate mass production, the reported method[16,17] was simplified (Fig. 2-1). In a typical run, 3 g CF11 was immersed in deionized water for 4 h at room temperature (RT, 25 °C) and filtered to remove water, followed by successive solvent

exchange with methanol and DMAc, each for 2 h. Then, the activated cellulose was soaked in 47 g LiCl (8 wt%)-DMAc solution under the protection of a N_2 atmosphere. After mechanical stirring for 12 h, a clear cellulose solution was obtained. To complete the dissolution of cellulose, the solution was kept overnight at 4 °C.[16] Finally, a transparent cellulose solution with 6 wt% concentration was obtained. The solution was stored at 4 °C until use. For concentrations below 6 wt%, the solution became clear only after stirring for several hours. With respect to 8 wt%, 24 h were needed for complete dissolution. According to the same procedure, 6 wt% of Merck and 6 wt% of Avicel cellulose solutions were obtained. The dissolution time was less than 2 h for both samples. On the contrary, even for 1 wt% BC solution, the dissolution took at least 24 h, and the viscosity of the solution was higher than the other samples.

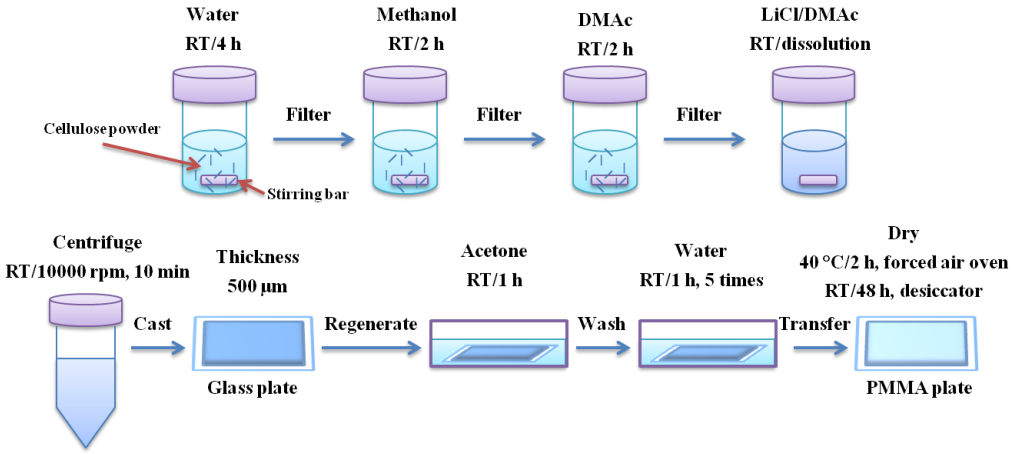

Figure 2-1. Scheme of the fabrication of cellulose film

2.2.3 Preparation of cellulose film

The cellulose solution was degassed by centrifugation at 10 000 rpm for 10 min at RT, then cast on a glass plate. The thickness was controlled at 0.5 mm using an applicator. After the glass plate was gently immersed into 100 ml of acetone bath, a

transparent cellulose gel was immediately formed. The cellulose gel was kept in acetone for 1 h, and washed with 100 ml deionized water five times to remove the salt completely, each time for 1 h. For the preparation of cellulose films, the usability of various kinds of organic solvents other than acetone was checked as regeneration solvents, with water, methanol, and ethanol. The washed sample was fixed on the poly(methyl methacrylate) (PMMA) plate with adhesive tape to prevent shrinkage[10] and was then dried in the oven at 40 °C for 2 h. The glass and Teflon plates were also employed as the substrate for this drying process (Fig. 2-1). The sample was further dried in a desiccator containing phosphorus(V) oxide at RT for at least 48 h. Finally, for 6 wt% of CF11 solution, a transparent cellulose film was obtained with a thickness of about 22 μm. In the following content, the samples prepared from different kinds and concentration of cellulose solutions are referred to as CF11 4%, CF11 5%, CF11 6%, CF11 7%, CF11 8%, Merck 6%, Avicel 6%, and BC 1%, respectively.

2.2.4 Enzymatic hydrolysis of CF11 6% and cellophane

CF11 6% and cellophane with similar thicknesses of 22-23 μm were treated with cellulolytic enzymes. Hydrolysis experiments were run concurrently. To minimize the difference in specific area, CF11 6% and the cellophane were cut into square shapes with the same size of about 2 cm × 2 cm. For each film, 150 mg of sample, 10 ml of sodium citrate buffer solution (0.05 M, pH 4.8), and 20 mg of cellulase were added in this order to a 50 ml vial. The vials were capped and put into a bioshaker at 40 °C with a shaking speed 200 rpm. To monitor the content of released reducing sugar, 100 μl of the supernatant was transferred from the vial to a test tube periodically and diluted with 2.9 ml of Milli-Q water, followed by blending with 3 ml of DNS reagent, which was

prepared according to the method reported by Miller.[30] The test tubes were heated in a boiling water bath for 15 min. After the development of color, 1 ml of 40 wt% Rochelle salt solution was added immediately. The test tubes were rapidly cooled down to RT using running water. The absorbance of the solution was measured at 575 nm using a Hitachi U2810 UV-visible spectrophotometer. Finally, the released reducing sugar content was calculated as D-glucose.

2.2.5 Characterization

Fourier transform infrared (FT-IR) spectra in the attenuated total reflection (ATR) mode were recorded on a Nicolet iS5 FT-IR Spectrometer with iD5 ATR accessory (Thermo Fisher Scientific Inc., Waltham, MA, USA). The optical transmittance of the films were measured from 200 to 900 nm using a Hitachi U2810 UV-visible spectrophotometer. Scanning electron microscopy (SEM) analysis was carried out by a HITACHI SU-3500 instrument (Hitachi High-Technologies Corp., Tokyo, Japan). Wide-angle X-ray diffraction (XRD) was performed on an X-ray diffractometer (Shimadzu XRD-6100) at a rate of 2° (2θ) min^{-1} over the 2θ range from 5° to 40°. The X-ray radiation used was Ni-filtered CuKα with a wavelength of 0.15406 nm. The voltage and current were set at 40 kV and 30 mA, respectively. Solid-state ^{13}C-NMR spectra with cross polarization/magic angle spinning (CP/MAS) were recorded on a 600 MHz NMR spectrometer (150.95 MHz for ^{13}C, Advance III, Brucker BioSpin GmbH, Rheinstetten, Germany) at RT. The chemical shift was calibrated by the carbonyl carbon of glycine at 176.46 ppm. The cellulose distribution in cellulose films was observed by an X-ray computed tomography (XCT) instrument at 80 kV and 100 μA with an isotropic voxel of 600 nm (SKY Scan 1172, High resolution

micro-CT, Brucker AXS GmbH, Karlsruhe, Germany). The tensile properties were measured by a Shimadzu EZ Graph instrument equipped with a 500 N load cell (Shimadzu Corp., Kyoto, Japan). A cross-head speed of 1 mm min^{-1} was used. The sample was cut into rectangular strips of 40 mm × 5 mm and tested with a span length of 10 mm.

2.3 Results and discussion

2.3.1 Characterization of cellulose film

To prepare cellulose film with a good appearance, three substrates were employed during the drying process (Fig. 2-1). The film was well attached to the glass plate, but the bonding force between the surfaces was so strong that the film could not be peeled off from the plate. In contrast, the bonding force between the film and Teflon was too weak to maintain the shape of the film, which was easily deformed after drying. The best result was obtained by using the PMMA plate. The bonding force between the surfaces was strong enough to fix the cellulose film. Meanwhile, the film can be easily detached from the plate. Considering the cost and environmental friendliness, four common solvents: water, methanol, ethanol, and acetone, were chosen as the regeneration solvents. The first three kinds of solvents caused a drastic shrinkage of the cellulose film. Only in the case of acetone, however, was a transparent, flat and smooth cellulose film obtained. The usability of acetone as a regeneration solvent has been previously reported,[6,31] but no description about the preparation of transparent films has been noted using the LiCl-DMAc solvent system. In addition, it was reported that acetone will lead to a better amorphous cellulose structure.[14] Based on the above reasons, acetone was chosen as the regeneration solvent. All of the cellulose films

regenerated individually from CF11, Merck, Avicel, and BC cellulose solutions in LiCl-DMAc by acetone possessed good optical appearance. Among them, CF11 6% was taken as a typical example, and its image is shown in Fig. 2-2.

Figure 2-2. Photo of transparent film of CF11 6%

A smooth and dense surface was observed by SEM in the micron level (Fig. 2-3). The thickness of the cellulose films increased with the increasing concentration of cellulose solution from 4 wt% to 7 wt% (16, 18, 22, and 29 μm, respectively), and a slight decrease appeared at 8 wt% (27 μm), because of the incomplete dissolution of cellulose into the solvent.

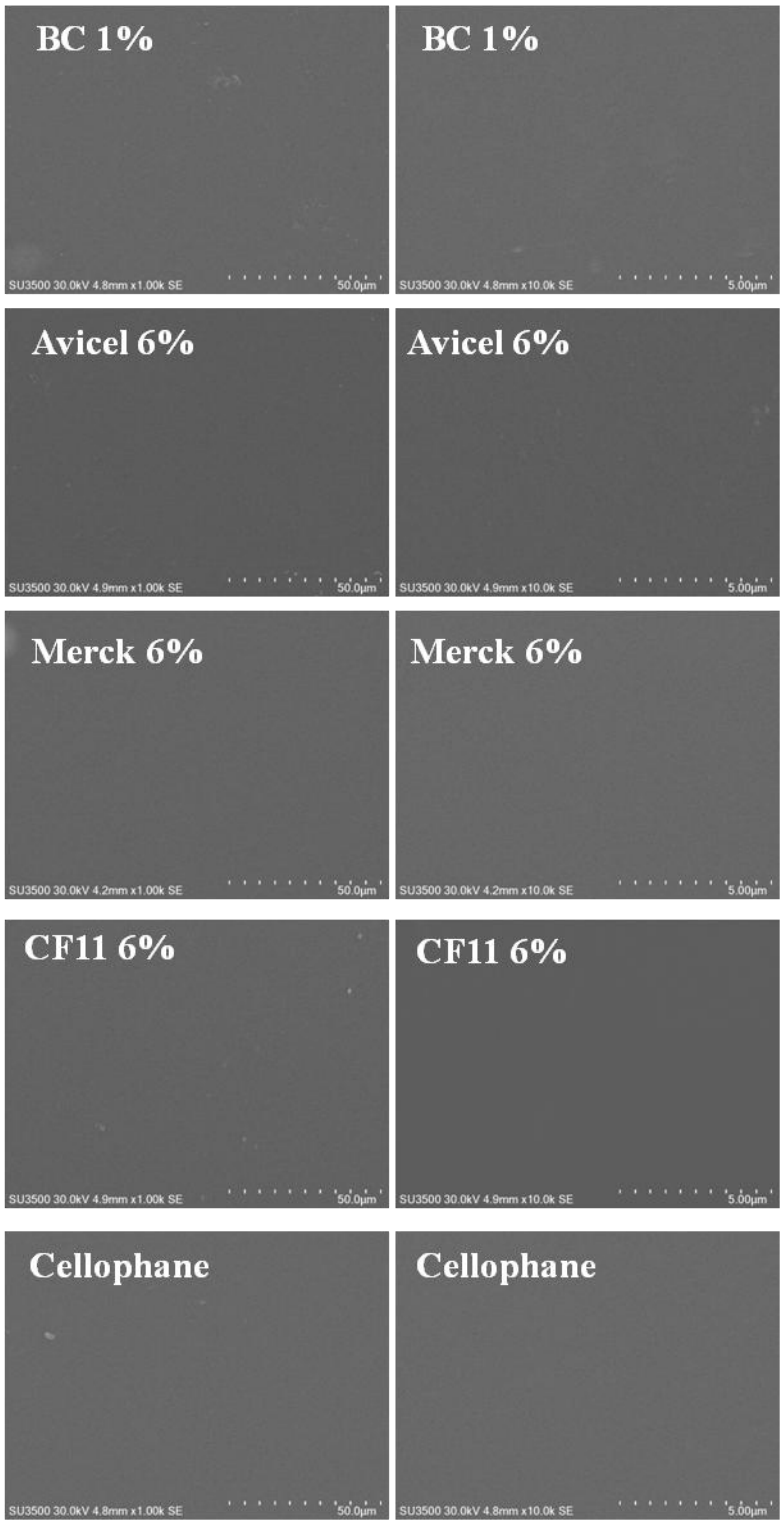

Figure 2-3. SEM micrographs of the surface of BC 1% film, avicel 6% film, merck 6% film, CF11 6% film, and Cellophane.

The crystalline structure of the native CF11, Merck, Avicel, and BC samples

was studied by XRD (Fig. 2-4a). The typical diffractions due to I_β-rich natural cellulose for the former three were observed at 2θ = 14.8°, 16.3°, and 22.6°, which corresponded to the $(1\bar{1}0)$, (110), and (200) planes,[32] respectively. In the case of I_α-rich BC, three distinct diffractions (100), (010), and (110) were observed at 2θ = 14.6°, 16.9°, and 22.7°, respectively.[29] After regeneration, these diffractions disappeared, showing a broad peak at $2\theta \approx$ 20° (Fig. 2-4b), which indicated that the cellulose I structure was transformed to amorphous cellulose during the dissolution, regeneration, and drying process. Compared to Ball-mill cellulose, the regenerated samples showed similar diffractions, except that, for Avicel 6%, there were weak peaks appearing at around 2θ = 12.1° and 22.0°. These diffractions were attributed to the cellulose II structure, indicating that a small amount of the cellulose II structure was also formed apart from just amorphous cellulose.

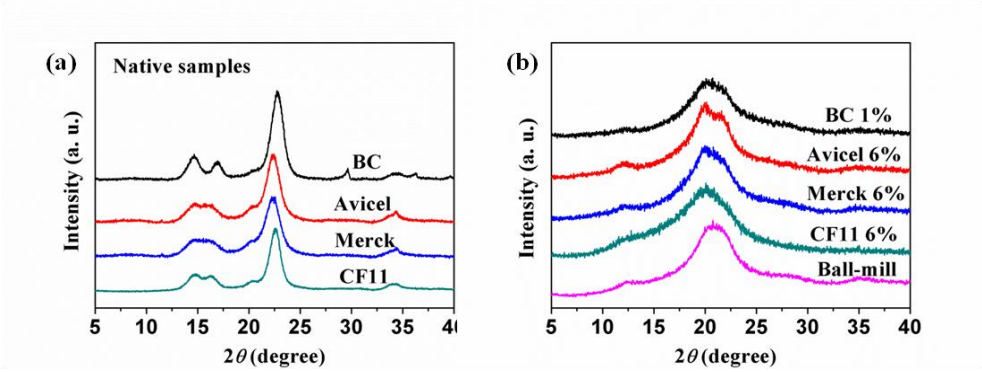

Figure 2-4. X-ray diffractions of (a) native samples, (b) regenerated samples and ball-milled sample.

The amorphous structure of the cellulose films was further confirmed by CP/MAS ^{13}C-NMR (Fig. 2-5). The native cellulose showed characteristic signals assignable to cellulose I (Fig. 2-5a): the signals around 105 ppm were assigned to the most deshielded anomeric carbon atom C1; the sharp signal at 89 ppm and the broad signal between 86 ppm and 80 ppm were assigned to C4 in the crystalline and

amorphous regions, respectively; the signals from 79 ppm to 70 ppm belonged to C2, C3, and C5; similar to C4, C6 displayed a sharp signal at 65 ppm and a broad signal around 63 ppm, corresponding to the crystalline and amorphous regions, respectively.[33] After regeneration (Fig. 2-5b), all the signals showed a decrease in sharpness, especially for C4. The sharp peaks at 89 ppm totally disappeared for CF11 6%. With respect to the other regenerated samples, only two small signals appeared in this area because of the regeneration of a small amount of the cellulose II structure. Moreover, the strength of signals from 86 ppm to 80 ppm increased for all samples. These changes stemmed from the differences between the crystalline and amorphous structure, including conformational differences, differences in bond geometries, and non-uniformities of the neighboring chain environments.[34] The results for the regenerated samples were similar to the ball-milled sample, indicating that highly amorphous cellulose films were obtained. Moreover, for CF11, the transformation from cellulose I to amorphous cellulose was more completely achieved by regeneration from the LiCl–DMAc solution, compared to the ball-milling method, since there were still two small signals around 89 ppm displayed for the ball-milled sample, due to the remaining cellulose I structure.

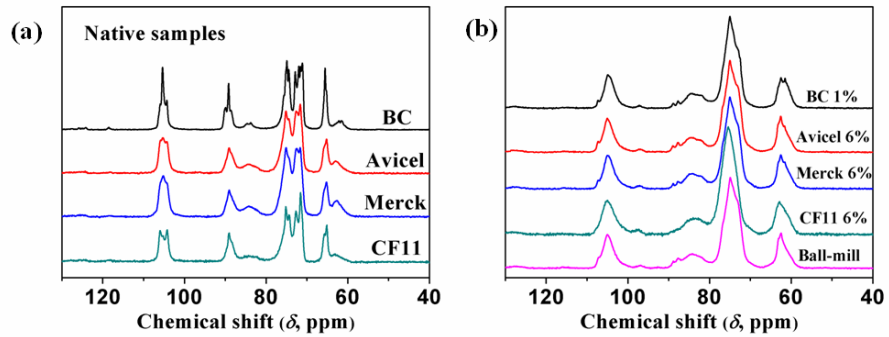

Figure 2-5. CP/MAS ^{13}C-NMR spectra of (a) native samples, (b) regenerated samples and ball-milled sample

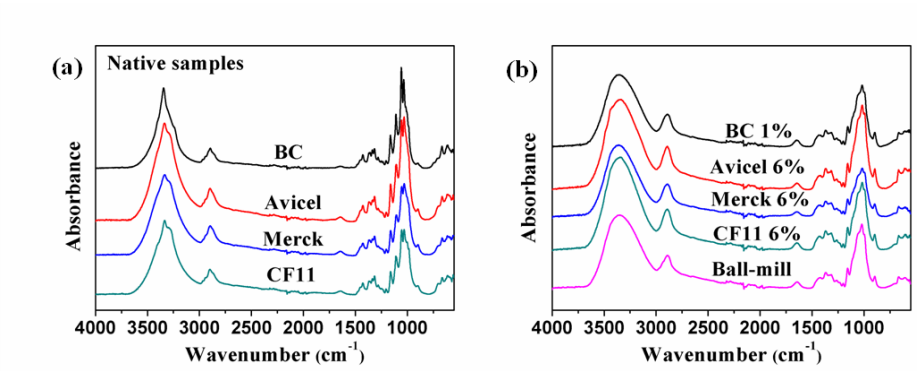

Figure 2-6. FT-IR spectra of (a) native samples, (b) regenerated samples and ball-milled sample

The FT-IR results (Fig. 2-6) also provided evidence of the transformation from the crystalline to the amorphous structure. The absorption at 1429 cm^{-1} was assigned to the CH_2 symmetrical bending vibration, and the absorption at 897 cm^{-1} responded to the change in molecular conformation due to rotation about the β-(1 → 4)-D-glucosidic linkage.[35] Normally, these two bands were used to measure the crystallinity of cellulose. In the native cellulose (Fig. 2-6a), a sharp absorption at 1429 cm^{-1} and a weak band at 897 cm^{-1} appeared. In the regenerated cellulose film (Fig. 2-6b), on the other hand, only a broad absorption at 1429 cm^{-1} could be seen and the intensity of the absorption at 897 cm^{-1} increased, proving the low crystallinity of the regenerated film. In addition, the intensity of the other peaks at 1335, 1315, 1111, 1057, and 1033 cm^{-1} decreased after the regeneration. The broad absorption in the 3600–3000 cm^{-1} region, due to the OH–stretching vibration, could reflect changes of the hydrogen bonds. A narrow peak appeared at 3340 cm^{-1} for native cellulose, which was caused by the regular arrangement of intramolecular and intermolecular hydrogen bonds. After regeneration, the regularity of hydrogen bonds was disturbed, and the peak shifts to a higher wavenumber at 3350 cm^{-1} and broadening were also detected. Since it was reported that unbounded or "free" OH groups absorb infra-red light at 3584 to 3650 cm^{-1},[36] which

was higher than that observed in the prepared films, we could conclude that the hydroxyl groups in the amorphous structure existed in an irregular arrangement of hydrogen bonds rather than in the free mode.

All of the cellulose samples, namely CF11, Merck, Avicel, and BC, could be transformed from cellulose I to a highly amorphous structure. Among these, the best result was obtained with CF11, whereas there was only a small amount of cellulose II structure regenerated in the case of Merck, Avicel, and BC. Therefore, in the following content, the properties of the ACF derived from CF11 were investigated and compared with those of cellophane.

2.3.2 Mechanism of the formation of ACF

Cellulose is mainly composed of two parts, namely, crystalline and disordered regions (Fig. 2-7). In most cases, the latter is referred to as "amorphous". Compared to the amorphous parts, the crystalline structure is more difficult to access and is the main obstacle to dissolution. First, water is used to swell the crystalline lattice, making the LiCl-DMAc solvent easy to penetrate. During the dissolution process, the $[DMAc_n + Li]^+$ macrocation is evolved, leaving the chloride anion (Cl^-) free, which disturbs the intermolecular and intramolecular hydrogen bonds by forming new hydrogen bonds with the hydroxyl groups of the cellulose chain.[20] Afterwards, the cellulose chains become much easier to tear off from the crystalline lattice and drag into solution. This process is repeated until the "true" solution is formed, in which the cellulose chains are freely extended, unlike in the other kinds of solvents such as aqueous NaOH/urea.[37] When this cellulose solution is immersed into a poor solvent, cellulose is immediately reprecipitated from the solution through the entanglement of the molecular

chains, leading to the formation of cellulose gel. Followed by the drying process, water quickly evaporates accompanying the collapse of the pores in the hydrogel, due to the high surface energy of water. In addition, regeneration of the hydrogen bonds between the cellulose chains provides another driving force. Finally, ACF with a dense structure was obtained. Although cellulose II is thermodynamically more stable, the drying process is so fast that the kinetic control takes advantage, and not enough time is left to rearrange the cellulose chains, which are more likely aligned in a bent and twisted conformation. A large amount of intramolecular hydrogen bonds replace the intermolecular hydrogen bonds existing in native cellulose to stabilize this conformation, making the ACF stable in common conditions unless exposed to high temperature, moisture, or pressure.

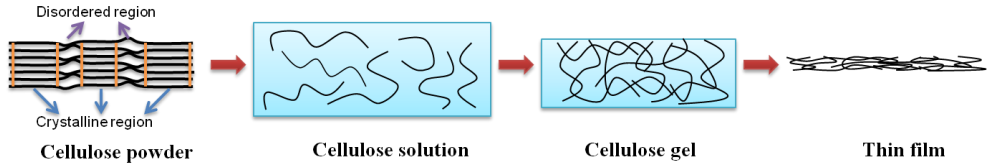

Figure 2-7. Scheme of the formation of ACF

The influence of the cellulose resources on its solubilization and formation of the amorphous structure is worth mentioning. Three plant celluloses with different particle sizes (CF11 > Merck > Avicel) were chosen. According to the XRD (Fig. 2-4) and ^{13}C-NMR (Fig. 2-5) results, the sequence of the perfection of the amorphous structure was CF11 > Merck > Avicel, which is consistent with their particle size. To some extent, particle size is related with the molecular chain length or degree of polymerization (DP). In the case of Avicel, the short chain length causes a large specific surface area contactable with the solvent, which promotes their high mobility leading

them to form the thermodynamically favored cellulose II structure during the regeneration and drying process. With respect to BC, because of its distinct complex entangled structure, the solubilization is difficult. Moreover, the viscosity of solution is obviously higher than those of the other three plant celluloses, reflecting the longest chain length of BC among the chosen cellulose resources. The molecular chains of BC probably still remain orientated, to some extent, in the solubilized state, which easily leads to the formation of the crystalline structure. Therefore, only for the sample with a median particle size, such as CF11, more perfect amorphous structure could be obtained.

2.3.3 Transparency of CF11 and cellophane

The transparency of cellulose films was investigated by UV-visible spectroscopy. All of the cellulose films from CF11 4% to CF11 8% possessed high transparency, not only in the visible region (transmittance is about 90%), but also in the near ultraviolet region (transmittance is above 70%), which was better than the commercial cellophane (Fig. 2-8) and other cellulose films.[6,38-39]

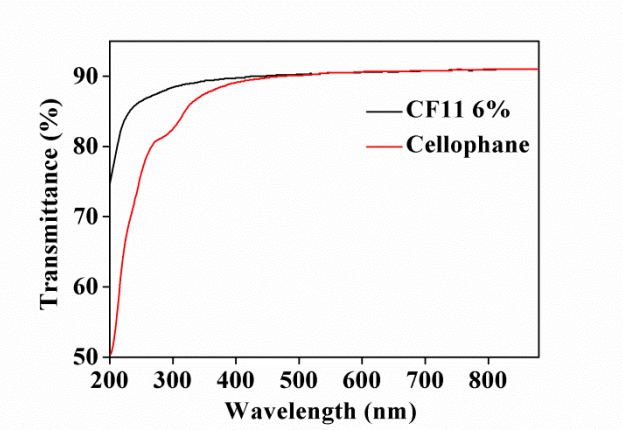

Figure 2-8. Transmittance of CF11 6% and Cellophane at UV-visible wavelength region.

The reason may be due to the difference of the crystalline structure between CF11 films and cellophane, the latter being characterized as cellulose II by XRD (Fig. 2-9a) and ^{13}C-NMR spectra (Fig. 2-9b).

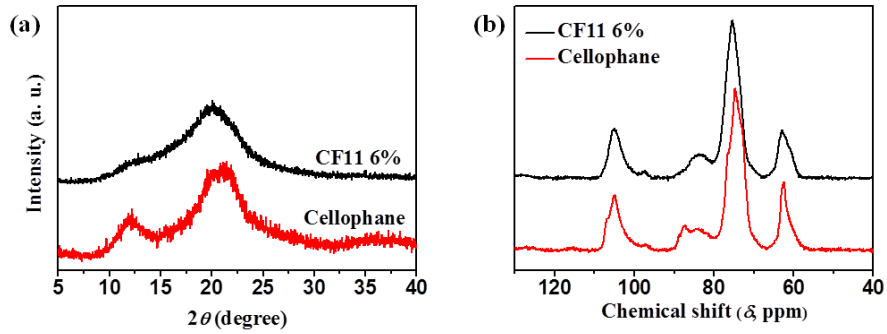

Figure 2-9. (a) X-ray diffractions of CF11 6% and Cellophane; (b) CP/MAS ^{13}C-NMR spectra of CF11 6% and Cellophane.

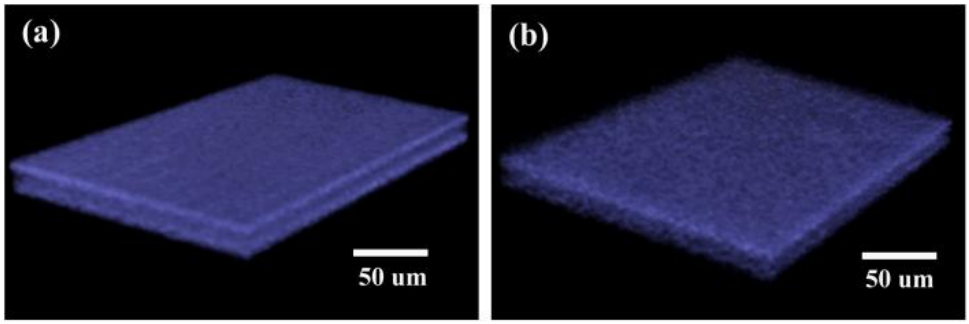

Figure 2-10. XCT image of (a) CF11 6% and (b) Cellophane

To further investigate the reason, XCT was measured, as it was recently used in the cellulose materials area.[40-42] With the help of XCT, a volumetric map of the specimen in three dimensions could be obtained. Meanwhile, the distribution of different components and pores could be differentiated. As the XCT images (Fig. 2-10) showed, CF11 6% was more homogeneous compared with cellophane, in the order of ≥600 nm. In the latter case, the presence of cloudy aggregates that may be composed of

the small crystal grains could be clearly detected. Such aggregates would cause the scattering of light, resulting in the inferior transparency of cellophane.

2.3.4 Mechanical properties of CF11 and cellophane

The tensile properties of cellulose films were investigated. For reference, cellophane was tested. Fig. 2-11 shows the typical stress–strain curves of cellulose samples. Table 2-1 summarizes the tensile properties of the measured samples.

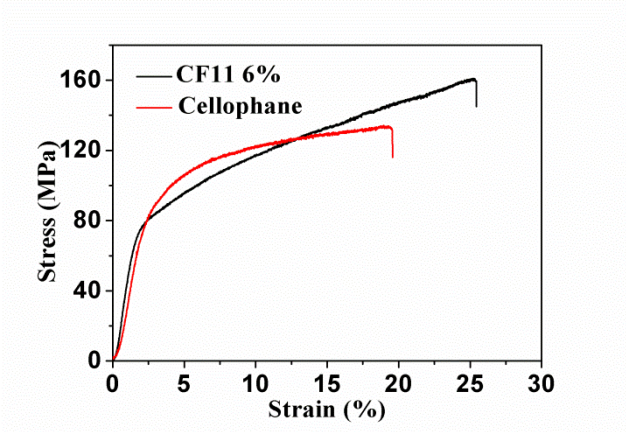

Figure 2-11. Stress-strain curves of CF11 6% and Cellophane.

Table 2-1. Tensile properties of ACFs and cellophane.

	ACF 4%	ACF 5%	ACF 6%	ACF 7%	ACF 8%	Cellophane
Elongation (%)	15.9 ±1.1*	20.7 ±1.2	23.9 ±3.2	22.5 ±2.2	17.6 ±3.3	19.9 ±3.7
Max stress (MPa)	132 ±7	161 ±8	157 ±8	145 ±9	145 ±9	135 ±6

*Standard deviation (SD). For each group experiment, 10 samples were tested and at least 3 samples were chosen.

The elongation at break and maximum stress for CF11 4% were 15.9% and 133 MPa, respectively. With the increasing concentration of the cellulose solution, the

elongation at break increased. After the maximum value of 23.9% was obtained for CF11 6%, an obvious decrease was shown for CF11 8%, because of the incomplete dissolution of cellulose, which was confirmed by the XRD results. The undissolved grain will function as a defect and is detrimental to the tensile performance. The largest maximum stress value was about 160 MPa, belonging to CF11 5% and CF11 6%. Because CF11 6% and cellophane possess similar thicknesses, the tensile properties of them were compared. The elongation at break (23.9%) and the maximum stress (157 MPa) of CF11 6% were higher than those of cellophane (19.9% and 135 MPa, respectively). Although the cellulose resource would affect the mechanical properties, such a rarely reported performance is probably attributed to the distinctive amorphous structure of ACF. In the amorphous structure, cellulose chains are assumed to be bent and twisted, intermolecular hydrogen bonds are ripped off and regenerated under stretching, leading to the extension and rearrangement of cellulose chains in a regular way, and ultimately a higher elongation at break and maximum stress are desirably obtained.

2.3.5 Enzymatic hydrolysis of CF11 6% and cellophane

The results of the enzymatic hydrolysis of CF11 6% and cellophane are shown in Fig. 2-12. In the initial 8 h, the concentration of the reducing sugar released by CF11 6% rapidly rose to 3.7 mg ml^{-1}, showing a little lower rise in the following time. After 48 h, the concentration increased up to 11.9 mg ml^{-1}. Assuming that the released reducing sugar was only comprised of glucose, it can be calculated that about 107 mg of CF11 6% (71.5% of the total amount) was hydrolyzed. Moreover, it was observed that CF11 6% was partially hydrolyzed into small pieces after 48 h. In contrast, the

concentration of reducing sugar released by cellophane rapidly increased to 1.0 mg ml^{-1} in the initial 4 h, showing only a small increase to 1.7 mg ml^{-1} after 48 h. About 15.0 mg of cellophane (10.0% of the total amount) was hydrolyzed. In addition, the films remained intact. The enzymatic hydrolysis rate of CF11 6% was above 7 times higher than that of cellophane.

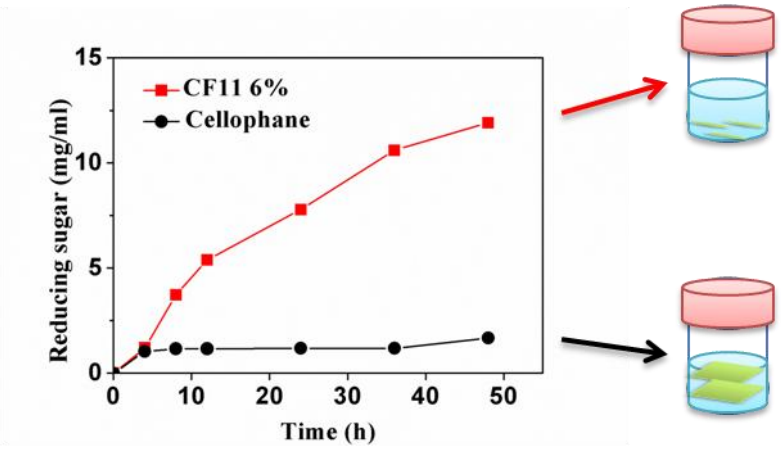

Figure 2-12. Time course of enzymatic degradation of CF11 6% and Cellophane

To explain this phenomenon, the mechanism of enzymatic hydrolysis would be focused (Fig. 2-13). Generally, the activity of cellulolytic enzymes largely depends on their types (*endo*- and *exo*-glucanases) and accessibility on the surface of cellulose as a subtrate.[43,44] Usually cellulase derived from *Trichoderma* and *Aspergillus* spp. are used for the degradation of natural cellulose I and more soft cellulosic materials, respectively. Here a cellulase originated from *Aspergillus niger* for testing the biodegradability of cellulose films was selected. For the cellophane (cellulose II), only cellulose chains on the surface are available for the attachment of the cellulase, since cellulose chains stack closely, and the film will be decomposed layer by layer. This process will greatly inhibit the hydrolysis of cellophane. The rapid increase in the beginning is attributed to the

amorphous region in the surface of cellophane. With respect to CF11 6%, cellulase does not only function on the surface but also acts on internal chains because of their more open and accessible structure. Under similar conditions, CF11 6% will provide more active sites and chain ends for attack by cellulase. Eventually, CF11 6% shows a higher efficiency of enzymatic hydrolysis. Therefore, it is reasonable to conclude that CF11 6% will be decomposed much faster in the natural world and be friendlier to the environment than cellophane or other crystalline types of cellulose products. Moreover, cellulosic waste derived from ACF can be recycled and converted to liquid fuels,[45] due to its higher efficiency of enzymatic hydrolysis compared to the other cellulose resource, which will completely release the burden to the environment.

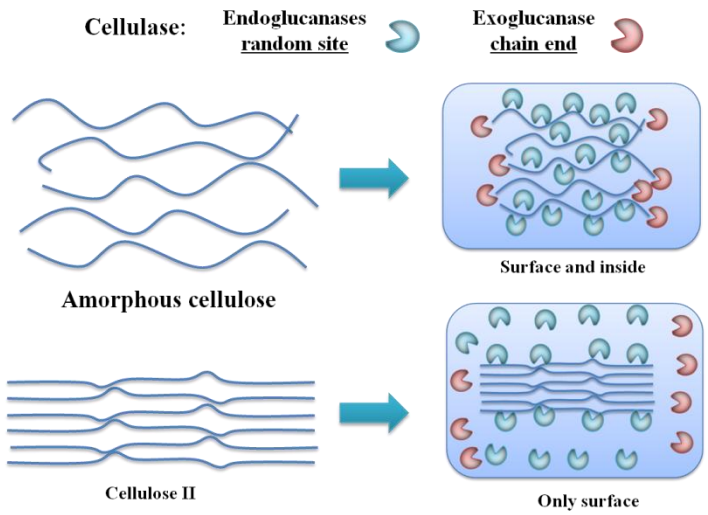

Figure 2-13. Mechanism of enzymatic degradation of CF11 6% and Cellophane

2.4 Summary

Cellulose films with excellent transparency were regenerated from LiCl-DMAc solutions by using acetone as the regeneration solvent. The cellulose films were highly amorphous, which was confirmed by XRD, ^{13}C-NMR, and FT-IR measurements.

According to the best of our knowledge, this was the first time that one had prepared such amorphous cellulose films with good performance through a simple, less-destructive, and universal method. Compared with commercial cellophane, ACF possessed a comparable mechanical performance, but much faster enzymatic hydrolysis rate, due to its distinctive amorphous structure, which is more open and accessible, indicating its prevailing environmental friendliness. Based on the present results, it can be concluded that the ACF possesses a great potential for replacing cellophane used in packaging materials. Moreover, it has importance to serve as a new standard sample for the study of cellulose structure and enzyme activity.

2.5 References

(1) Yano, S.; Hatakeyama, H.; Hatakeyama, T. *J. Appl. Polym. Sci.* **1976,** *20,* 3221-3231.

(2) Rinaldi, R.; Schüth, F. *ChemSusChem* **2009,** *2,* 1096-1107.

(3) Dadi, A. P., Varanasi, S.; Schall, C. A. *Biotechnol. Bioeng.* **2006,** *95,* 904-910.

(4) Bertran, M. S.; Dale, B. E. *Biotechnol. Bioeng.* **1985,** *27,* 177-181.

(5) Fan, L. T.; Lee, Y.-H.; Beardmore, D. H. *Biotechnol. Bioeng.* **1980,** *22,* 177-199.

(6) Yang, Q.; Fukuzumi, H.; Saito, T., Isogai, A.; Zhang, L. *Biomacromolecules* **2011,** *12,* 2766-2771.

(7) Fink, H. P.; Weigel, P.; Purz, H. J.; Ganster, J. *Prog. Polym. Sci.* **2001,** *26,* 1473-1524.

(8) Qi, H.; Chang, C.; Zhang, L. *Green Chem.* **2009,** *11,* 177-184.

(9) Hermans, P. H.; Weidinger, A. *J. Am. Chem. Soc.* **1946,** *68,* 2547-2552.

(10) Manley, R. S. J. *J. Polym. Sci., Part A: General Papers* **1963,** *1***,** 1893-1899.

(11) Jeziorny, A.; Kepka, S. *J. Polym. Sci., Part B: Polym. Lett.* **1972,** *10***,** 257-260.

(12) Jeffries, R. *J. Appl. Polym. Sci.* **1968,** *12,* 425-445.

(13) Schroeder, L. R.; Gentile, V. M.; Atalla, R. H. *J. Wood Chem. Technol.* **1986,** *6,* 1-14.

(14) Isogai, A.; Atalla, R. H. *J. Polym. Sci., Part A: Polym. Chem.* **1991,** *29***,** 113-119.

(15) El-Kafrawy, A. *J. Appl. Polym. Sci.* **1982,** *27,* 2435-2443.

(16) Dupont, A. L. *Polymer* **2003,** *44,* 4117-4126.

(17) McCormick, C. L.; Callais, P. A.; Hutchinson, B. H. *Macromolecules* **1985,** *18,* 2394-2401.

(18) Striegel, A. M. *J. Chil. Chem. Soc.* **2003,** *48,* 73-77.

(19) Potthast, A.; Rosenau, T.; Buchner, R.; Röder, T.; Ebner, G.; Bruglachner, H.; Sixta, H.; Kosma, P. *Cellulose* **2002,** *9*, 41-53.

(20) Dawsey, T. R.; McCormick, C. L. *J. Macromol. Sci., Polym. Rev.* **1990,** *30***,** 405-440.

(21) Nishio, Y.; Manley, R. S. *Polym. Eng. Sci.* **1990,** *30*, 71-82.

(22) Nishio, Y.; Manley, R. S. *Macromolecules* **1988,** *21***,** 1270-1277.

(23) Nishio, Y.; Roy, S. K.; Manley, R. S. *Polymer* **1987,** *28*, 1385-1390.

(24) Zhang, X.; Zhu, J.; Liu, X.; Feng, J. *Cellulose* **2012,** *19*, 121-126.

(25) Zhang, X.; Zhu, J.; Liu, X. *Macromol. Res.* **2012,** *20*, 703-708.

(26) Zhang, X.; Liu, X.; Zheng, W.; Zhu, J. *Carbohydr. Polym.* **2012,** *88*, 26-30.

(27) Kim, J.-W.; Park, S.; Harper, D. P.; Rials, T. G. *J. Appl. Polym. Sci.* **2013,** *128*, 181-187.

(28) Gindl, W.; Keckes, J. *Polymer* **2005,** *46*, 10221-10225.

(29) Iwata, T.; Indrarti, L.; Azuma, J. *Cellulose* **1998,** *5*, 215-228.

(30) Miller, G. L. *Anal. Chem.* **1959,** *31*, 426-428.

(31) Geng, H.; Yuan, Z.; Fan, Q.; Dai, X.; Zhao, Y.; Wang, Z.; Qin, M. *Carbohydr. Polym.* **2014,** *102*, 438-444.

(32) Isogai, A.; Usuda, M.; Kato, T.; Uryu, T.; Atalla, R. H. *Macromolecules* **1989,** *22*, 3168-3172.

(33) Atalla, R. H.; Gast, J. C.; Sindorf, D. W.; Bartuska, V. J.; Maciel, G. E. *J. Am. Chem. Soc.* **1980,** *102*, 3249-3251.

(34) VanderHart, D. L.; Atalla, R. H. *Macromolecules* **1984,** *17*, 1465-1472.

(35) Nelson, M. L.; O'Connor, R. T. *J. Appl. Polym. Sci.* **1964,** *8*, 1311-1324.

(36) Kondo, T.; Sawatari, C. *Polymer* **1996,** *37*, 393-399.

(37) Cai, J.; Zhang, L. *Macromol. Biosci.* **2005,** *5*, 539-548.

(38) Nakagaito, A. N.; Nogi, M.; Yano, H. *MRS Bulletin* **2010,** *35*, 214-218.

(39) Nogi, M.; Iwamoto, S.; Nakagaito, A. N.; Yano, H. *Adv. Mater.* **2009,** *21***,** 1595-1598.

(40) Kastner, J.; Plank, B.; Salaberger, D., 18 World Conference on Nondestructive Testing, Durban **2012**

(41) Kastner, J.; Kickinger, Salaberger, R.; D. *J. Cell. Plast.* **2011,** *47*, 567-578.

(42) Faessel, M.; Delisée, C.; Bos, F.; Castéra, P. *Compos. Sci. Technol.* **2005,** *65*, 1931-1940.

(43) Zhang, Y.-H. P.; Lynd, L. R. *Biotechnol. Bioeng.* **2004,** *88*, 797-824.

(44) Teeri, T. T. *Trends Biotechnol.* **1997,** *15*, 160-167.

(45) Bayer, E. A.; Lamed, R.; Himmel, M. E. *Curr. Opin. Biotechnol.* **2007,** *18*, 237-245.

Chapter 3 Lipase-catalyzed synthesis of tri-branched poly(ricinoleic acid) and its application

3.1 Introduction

Trans-1,4-polyisoprene is a semicrystalline polymer, harder and less elastic than its stereoisomer *cis*-1,4,-polyisoprene (CPI, main component of natural rubber).[1,2] *Trans*-1,4-polyisoprene can be extracted from a small number of plant species, such as *Eucommia ulmoides, Palaquium gutta, Manilkara bidentata, Achras zapota, Garrya flavescens and Garrya wrightii*.[3-5] Among them, *Eucommia ulmoides* is extensively cultivated in China as a source of a Chinese traditional medicine.[5,6] Nowadays, there are several applications of natural *trans*-1,4-polyisoprene, e.g., golf balls and endodontic filling materials.[2,7]

In recent years, natural *trans*-1,4-polyisoprene extracted from *Eucommia ulmoides* Oliver (EuTPI) attracts the researchers' interests again due to the ever-increasing environmental awareness and fossil fuel crisis. Previously, the histochemical study of EuTPI accumulation in *Eucommia ulmoides* Oliver was conducted, revealing that EuTPI was initially synthesized as granules in non-articulated laticifers and changes form to fibers along with laticifer maturation.[3,6] A bio-based polymer was also developed with dynamically crosslinked network structure from EuTPI.[8] Zhang et al. studied the difference between EuTPI and synthetic *trans*-1,4-polyisoprene.[9] Yan and Xue et al. developed a series of patented products of EuTPI, and also studied damping properties of EuTPI and its blends with other elastomers.[10,11] Sarina et al. investigated the dynamic properties of EuTPI with different

degrees of crosslinking.[12]

One of the crucial problems of EuTPI would be poor processing ability, which hampers widespread applications. Unlike CPI, EuTPI with high molecular weight ($M_w > 10^6$)[8] did not flow and still possessed high modulus even above its melting point, which easily caused defects and failures during the extrusion and molding processes, eventually affected the performance and appearance of the products. Thus, the improvement of the processing ability of EuTPI becomes an urgent issue.

Applications of ricinoleic acid have been extensively studied due to its abundant resource, excellent biodegradability, and multi-functional groups.[13-26] Ricinoleic acid, taking up 90% of castor oil, possesses hydroxyl and carboxyl groups as well as C=C bond, making it polymerizable and crosslinkable.[14] Ebata et al. synthesized high molecular weight poly(ricinoleic acid) (PRA) from methyl ricinoleate (purity > 99%) using immobilized lipase as catalyst.[19] Such a polyester was a viscous liquid at room temperature, completely amorphous and biodegradable. Subsequently, they obtained a thermosetting elastomer from the vulcanization of PRA.[18] Roberson et al. prepared a poly(L-lactide) (PLLA)/PRA diblock copolymer as compatibilizer to improve the toughness of PLLA.[16] Lebarbe et al. prepared PLLA/PRA/PLLA triblock copolyester.[15] By incorporation of 17 wt% of the PRA block, the ultimate strain increased from 5% to 98%. Gautrot et al. synthesized a high molecular weight copolyester based on bile acid and ricinoleic acid via entropy-driven ring-opening metathesis polymerization.[17] The copolyester displayed tunable mechanical properties and heterogeneous degradation behaviors. The aforementioned researches incorporated flexible and amorphous properties of PRA into the rigid materials, such as PLLA and poly(bile acid). These previous studies inspire me to introduce PRA into EuTPI to

improve the properties.

Herein, two types of crosslinkable polyesters were synthesized, a linear PRA (LPRA) and a tri-branched PRA (BPRA), as additives for improvement of the properties of EuTPI. LPRA was synthesized from cost-effective ricinoleic acid with an immobilized lipase as catalyst. Similarly, BPRA was synthesized using castor oil as molecular core (Fig. 3-1). Various amounts of LPRA and BPRA were separately introduced into EuTPI. The morphology, crystallization behaviors, thermal and rheological properties of the blend films were systematically investigated. This research aims to improve the processing ability of EuTPI by blending a crosslinkable polyester.

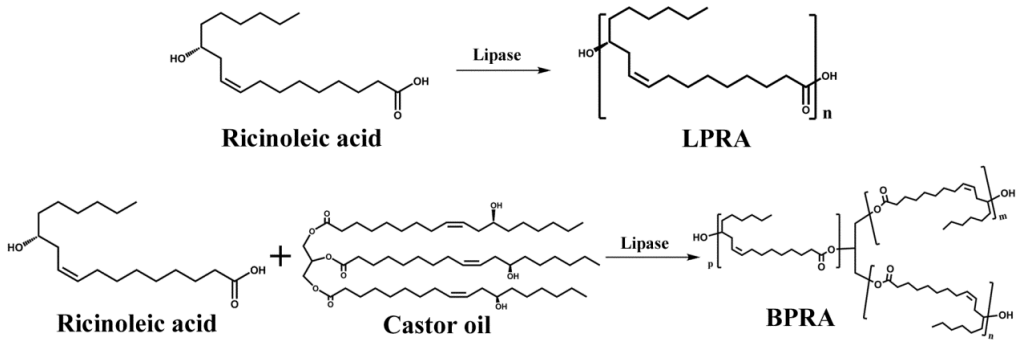

Figure 3-1. Scheme of lipase-catalyzed synthesis of LPRA and BPRA

3.2 Experimental procedure

3.2.1 Materials

Lipase (lipase PS IM Amano, immobilized on diatomaceous earth), ricinoleic acid (purity ≈ 80%), and castor oil were purchased from Wako Pure Chemical Industries, Ltd., Japan. Dicumyl peroxide (DCP) was purchased from Sigma-Aldrich. Molecular sieves 4 A 1/8 were purchased from Nacalai Tesque Inc., Japan, and activated in *vacuo* at 150 °C for 4 h before usage. All reagents without special mention were used as received.

EuTPI produced from the seeds of *Eucommia ulmoides* Oliver was supplied by Hitachi Zosen Co., Osaka, Japan, and purified according to the previous report.[8] Briefly, 5 g of crude sample was dissolved in 300 mL of toluene by vigorous stirring at 40 °C for 48 h. The undissolved impurity was removed by centrifugation. The pure EuTPI was obtained after evaporating the solvent under reduced pressure. Molecular weight of EuTPI (M_w = 1.2 × 10^6, PDI = 1.8) was characterized by size exclusion chromatographic (SEC) analysis.

3.2.2 Synthesis of LPRA

Ricinoleic acid (2.0 g, 6.7 mmol) was added in a 100 mL of tube. Lipase PS (0.60 g, 30 wt% for ricinoleic acid) pre-dried for 2 h *in vacuo* at room temperature was carefully added at the bottom of the tube.[19] The molecular sieves were sealed in the upper part of the tube (Fig. 3-2). The reaction was performed at 60 °C for 7 days. Then, 20 mL of chloroform was added to dissolve the product, followed by filtration to remove lipase PS. The solution was concentrated under reduced pressure and the concentrate was dropped in 20 mL of methanol to remove the unreacted monomer and oligomer. The product precipitated at the bottom layer was collected and dried *in vacuo* at 60 °C until the weight was constant. The yield of LPRA was about 80%.

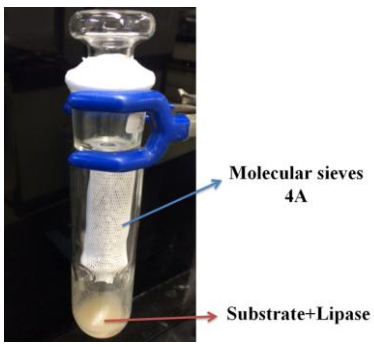

Figure 3-2. Reaction tube for lipase-catalyzed synthesis of LPRA and BPRA

3.2.3 Synthesis of BPRA

Ricinoleic acid (2.0 g, 6.7 mmol) and castor oil (0.16 g, 0.17 mmol) were added in a 100 mL of tube. The mixture was vigorously stirred at room temperature for 15 min. Polymerization was carried out as described above for the synthesis of LPRA by using the pre-dried lipase PS as catalyst (0.65 g, 30 wt% for the total weight of ricinoleic acid and castor oil) and the molecular sieves as a water scavenger. After the reaction, the crude product was isolated by solubilization in chloroform (20 mL), removal of lipase PS, and evaporation of the solvent under reduced pressure. The product was dissolved in 10 ml of acetone by gentle heating. Then, the solution was sealed and kept overnight in an ice-water bath. The formed precipitates at the bottom layer were collected. The purification procedures were performed twice. Finally, a transparent viscous liquid was obtained after drying to constant weight *in vacuo* at 60 °C. The yield of BPRA was about 70%.

3.2.4 Preparation of the films from EuTPI/LPRA and EuTPI/BPRA

Firstly, 0.050 g LPRA, 0.95 g EuTPI and 30 mL of chloroform were sequentially added in a 50 ml of vial. Then, the mixture was vigorously stirred for 24 h at room temperature, followed by casting the resulting solution to a Teflon mold and drying it for overnight. To completely remove the solvent, the sample was further dried *in vacuo* at room temperature for 24 h. Then, the sample was sandwiched by two stainless plates with a 100 μm of spacer. The hot-pressing process was performed at 100 °C under a pressure of 10 MPa for 10 min. Then, the film was naturally cooled down to room temperature. Finally, a blend film with 5 wt% of LPRA was prepared, which was referred as EuTPI-LPRA5%. According to the same procedure, EuTPI-LPRA10%,

EuTPI-LPRA15%, EuTPI-LPRA20%, EuTPI-BPRA5%, EuTPI-BPRA10%, EuTPI-BPRA15%, and EuTPI-BPRA20% were prepared. For comparison, the film from pure EuTPI was also prepared. The films were kept *in vacuo* for at least 24 h before any test.

The cured films were prepared using the similar procedures except for the addition of DCP (2.0 wt% for the total weight of BPRA and EuTPI) after EuTPI and BPRA were completely dissolved.[9] The films were hot-pressed at 150 °C under a pressure of 10 MPa for 30 min. The corresponding samples were referred as EuTPI-cured and EuTPI-BPRA15%-cured.

3.2.5 Characterization

^{1}H NMR spectra were recorded in $CDCl_3$ using a Bruker DPX-400 instrument (Bruker BioSpin Co., MA, USA). Fourier transform infrared (FT-IR) spectra in the attenuated total reflection (ATR) mode were recorded on a Nicolet iS5 FT-IR spectrometer with iD5 ATR accessory (Thermo Fisher Scientific Inc., Waltham, MA, USA). SEC was performed on a TOSOH SC-8020 apparatus equipped with refractive-index (RI) and UV detectors (Tosoh Co., Tokyo, Japan). Two groups of columns TSKgel GMH_{HR}-H (S) (for analysis of EuTPI) and TSKgel $G4000H_{XL}$ (for analysis of LPRA and BPRA) were used. Chloroform was used as an eluent at a flow rate of 1.0 mL/min at 40 °C. The molecular weight was calibrated by polystyrene standards. Thermogravimetric analysis (TGA) was conducted on a SII TG/DTA7200 (Hitachi High-Tech Science Co., Tokyo, Japan) from 40 °C to 500 °C at a heating rate of 10 °C/min under nitrogen. Differential scanning calorimetry (DSC) thermograms were measured using a SII DSC6220 equipment (Hitachi High-Tech Science Co., Tokyo,

Japan) under nitrogen. The samples were first heated up to 100 °C from room temperature and held for 5 min to eliminate the thermal history, then cooled down to -100 °C and held for 5 min, subsequently heated up from -100 °C to 100 °C. Both of the heating and cooling processes were operated at the same scanning rate of 10 °C/min. Scanning electron microscopic (SEM) analysis was carried out by a Hitachi SU-3500 instrument (Hitachi High-Technologies Co., Tokyo, Japan). Rheological measurements were performed on a Haake RheoStress 6000 Rheometer (Thermo Fisher Scientific Inc., Waltham, MA, USA) using 20 mm diameter of parallel plates. To ensure the adhesion of samples to the plates, 25 N of initial force was employed. A stress sweep test was initially performed to ensure that the stress used was within the linear viscoelastic range. Frequency sweeps were executed on each of samples over a frequency range of 0.1–100 rad/s at 80 °C.

3.3 Results and discussion

3.3.1 Structural characterization of LPRA and BPRA

LPRA was synthesized according to the reported method.[19] The degree of polymerization of LPRA was around 10, which was calculated from ^{1}H-NMR spectroscopic results (Fig. 3-3). For synthesis of BPRA, castor oil was used as multifunctional initiator, which is bio-based and well compatible with ricinoleic acid; castor oil possesses about 2.7 hydroxyl groups per molecule. The introduction of castor oil was expected to not only increase the molecular weight but also lead to a branched structure. To promote the reaction toward favored direction, the molar ratio between ricinoleic acid and castor oil was set as 40 to 1. By removing the unreacted monomer and oligomer, the product showed a unimodal peak in the SEC curve (Fig. 3-4). The

molecular weight was about 1.0×10^4 (PDI = 1.8), and higher than that of LPRA (M_w = 6.6×10^3, PDI = 2.5). In the ^{1}H-NMR spectrum of BPRA (Fig. 3-3), characteristic peaks derived from castor oil were found in the range from 4.0 ppm to 4.4 ppm (peaks d). From the ratio of the integrated area between these peaks and peak c due to ester bond at 4.9 ppm, it was confirmed that every branch of BPRA was composed of about 12 monomers.

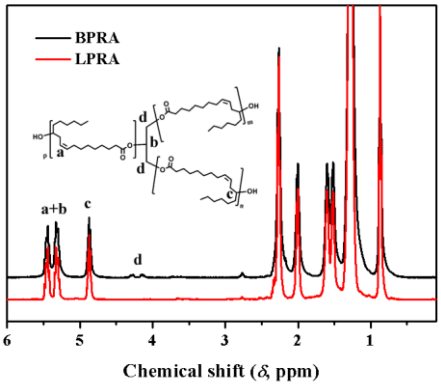

Figure 3-3. ^{1}H-NMR spectra of LPRA and BPRA

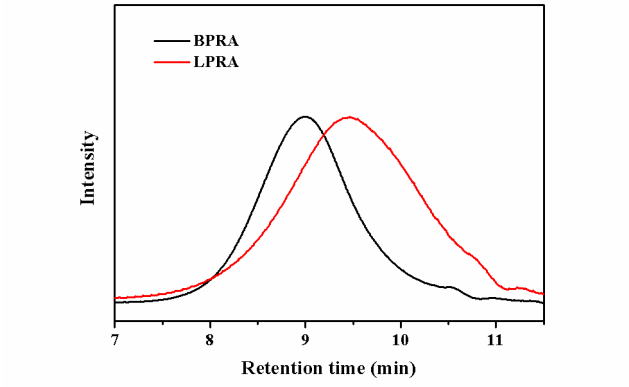

Figure 3-4. SEC curves of LPRA and BPRA

Moreover, the synthesis of LPRA and BPRA was confirmed by the FT-IR

spectroscopic analysis. The characteristic peaks of hydroxyl (3200 ~ 3650 cm^{-1}) and carboxylate (1710 cm^{-1}) groups found in the spectrum of ricinoleic acid disappeared in that of the product (Fig. 3-5 and Fig. 3-6), instead a strong peak owing to the ester carbonyl bond appeared at 1730 cm^{-1}. The above spectroscopic data clearly support the formation of BPRA.

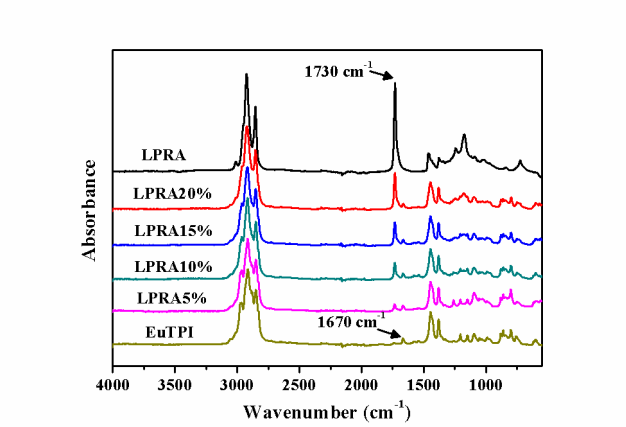

Figure 3-5. FT-IR spectra of LPRA, EuTPI, EuTPI-LPRA5%, EuTPI-LPRA10%, EuTPI-LPRA15%, and EuTPI-LPRA20%

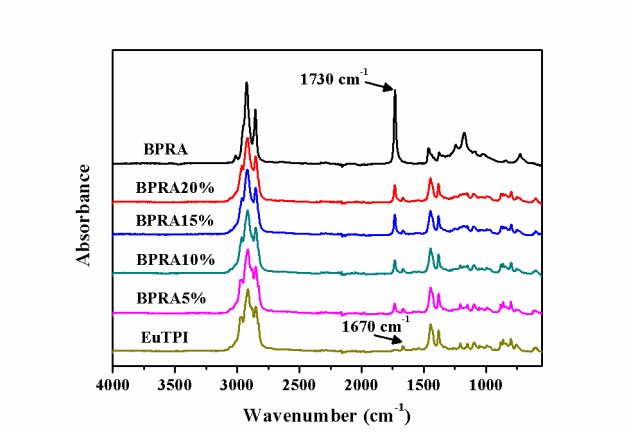

Figure 3-6. FT-IR spectra of BPRA, EuTPI, EuTPI-BPRA5%, EuTPI-BPRA10%, EuTPI-BPRA15%, and EuTPI-BPRA20%

3.3.2 Morphology of EuTPI, EuTPI/LPRA and EuTPI/BPRA blend films

LPRA and BPRA were separately introduced into EuTPI to examine their abilities for the improvement of EuTPI properties. For the EuTPI/LPRA blend films, uniform appearance was displayed when 5 wt% and 10 wt% of LPRA was introduced. With the increasing ratio of LPRA, the surface of the blend film became sticky, suggesting that macro-phase separation occurred. Fig. 3-7 shows the SEM images of the surface morphology of the EuTPI/LPRA blend films. For EuTPI-LPRA5%, small droplets with irregular shape in the EuTPI matrix were observed. As the mixed ratio of LPRA increased, the droplets coalesced and nonuniformly distributed in the matrix of EuTPI.

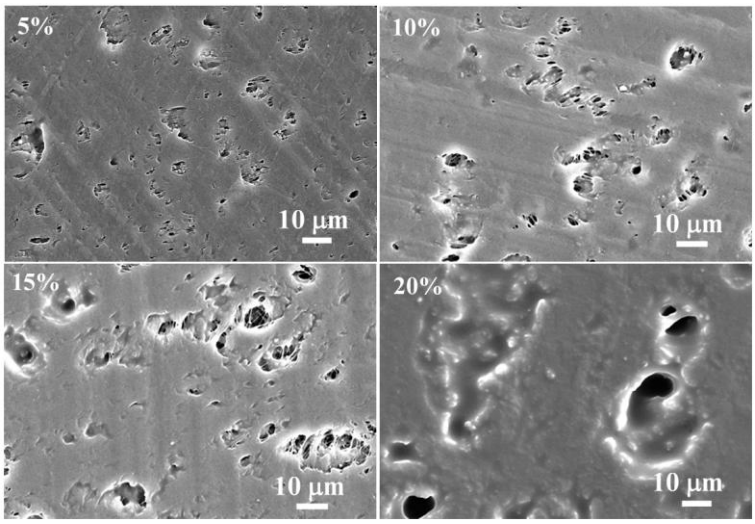

Figure 3-7. SEM micrographs of surface of EuTPI-LPRA5%, EuTPI-LPRA10%, EuTPI-LPRA15%, and EuTPI-LPRA20%

In contrast, all films consisting of EuTPI and BPRA showed uniform appearance and hard surface, suggesting that the macro-phase separation did not occur. Fig. 3-8 shows the SEM micrographs of pure EuTPI and EuTPI/BPRA blend films. In the case of Eu-BPRA5%, a similar morphology with pure EuTPI was shown, implying that BPRA was compatible with EuTPI. When 10 wt% of BPRA was added, small

droplets appeared and uniformly distributed in the EuTPI matrix. Up to 15 wt% of BPRA, the droplets still displayed uniform distribution with the increasing size of the droplets not only in the surface but also in the cross section. For EuTPI-BPRA20%, however, the coalescence became serious, and the droplets were nonuniformly distributed. Therefore, the mixing of 15 wt% BPRA should be the upper limitation for the blending. The above results indicate that BPRA possessed better compatibility with EuTPI than LPRA and could be uniformly distributed in the EuTPI matrix in the form of small droplets up to the content of 15 wt%. It was believed that the obvious differences between EuTPI/LPRA and EuTPI/BPRA blend films were caused by the different interfacial tension of EuTPI with LPRA and BPRA.[27] The branched structure and more terminal hydroxyl groups of BPRA with respect to LPRA would result in larger interfacial tension with EuTPI matrix. The large interfacial tension leaded to the formation of small droplets of BPRA, which could steadily and uniformly exist in the EuTPI matrix up to the content of 15 wt%. In contrast, LPRA with smaller interfacial tension easily coalesced and nonuniformly distributed in the EuTPI matrix.

The morphological change of the cured samples was investigated. Fig. 3-9 shows the surface morphology of the EuTPI-cured and EuTPI-BPRA15%-cured samples. EuTPI-cured displayed the surface morphology similar to that of the pure EuTPI sample without crosslinking (Fig. 3-8). For EuTPI-BPRA15%-cured, however, the uniform droplets disappeared, displaying the homogenous surface compared to that of EuTPI-BPRA15% without crosslinking. These SEM images suggest that BPRA was chemically incorporated to the crosslinked network of EuTPI through the reaction of the C=C bonds of EuTPI and BPRA. Compared to other common additive such as glycerol, BPRA was much more difficult to escape from the EuTPI matrix, leading to the more

stable performance of the final product.

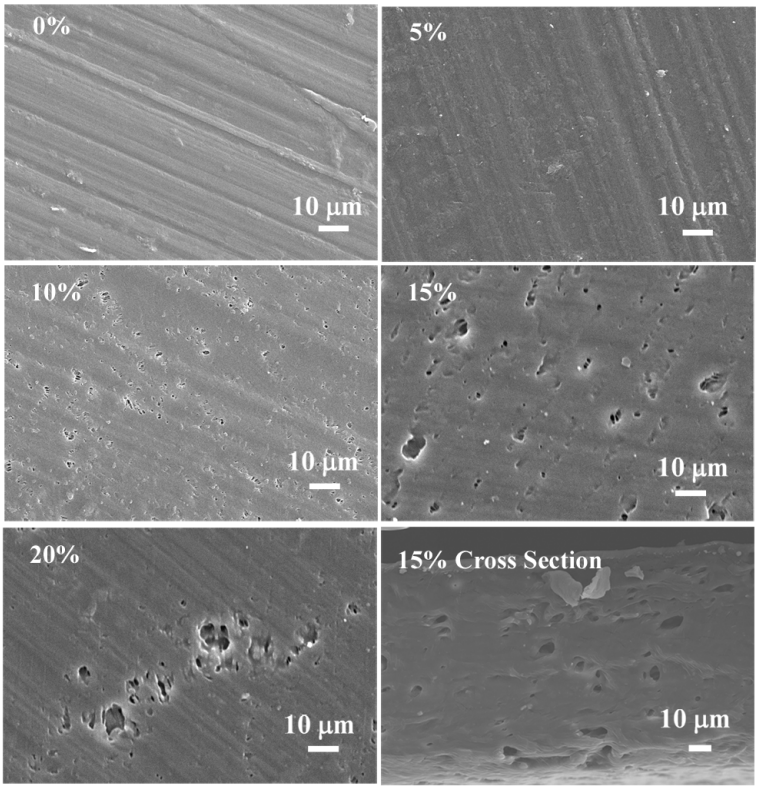

Figure 3-8. SEM micrographs of surface of EuTPI, EuTPI-BPRA5%, EuTPI-BPRA10%, EuTPI-BPRA15%, EuTPI-BPRA20%, and cross section of EuTPI-BPRA15%

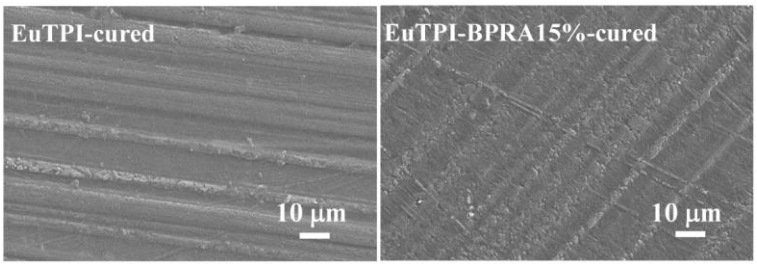

Figure 3-9. SEM micrographs of surface of EuTPI-cured and EuTPI-BPRA15%-cured

3.3.3 Rheology studies

The rheological properties of EuTPI, EuTPI/LPRA and EuTPI/BPRA blend films were studied by rheometer. Fig. 3-10 shows the results of EuTPI/LPRA blend

films. The storage modulus (G') and loss modulus (G'') of all films displayed plateaus across the entire frequency range (ω) from 0.1 to 100 rad/s at 80 °C, suggesting the strong entanglement of molecular chains. With the increasing content of LPRA, G', G'', and complex viscosity (η) showed decreased tendency. For EuTPI-LPRA20%, however, G' and η were abnormally higher than those of EuTPI-LPRA10% and EuTPI-LPRA15%, which is probably due to much more serious coalescence and nonuniform distribution of LPRA in the EuTPI matrix. For all EuTPI/LPRA blend samples, G' was higher than the corresponding G'', implying the elastic gel behavior of EuTPI/LPRA blend samples at 80 °C. These data indicate that LPRA was not effective to improve the processing ability of TPI.

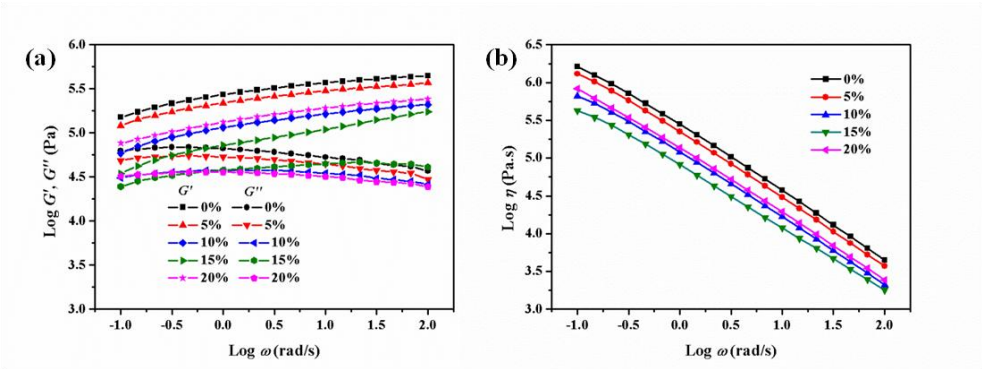

Figure 3-10. Rheological properties of EuTPI, EuTPI-LPRA5%, EuTPI-LPRA10%, EuTPI-LPRA15%, and EuTPI-LPRA20%: (a) frequency-dependent dynamic storage modulus *G'* and loss modulus *G''* curves; (b) frequency-dependent complex viscosity η curves

For EuTPI, EuTPI-BPRA5%, and EuTPI-BPRA10%, G' was higher than G'', and all of them showed plateaus across the entire frequency range (ω) from 0.1 to 100 rad/s at 80 °C (Fig. 3-11a). These results suggest the existence of the strong entanglement between molecular chains, which made samples behave like elastic gels and lost mobility even above the melting point of TPI. Below 10 wt% of BPRA, G', G'',

and η only displayed a slight decrease with the increasing content of BPRA. As for EuTPI-BPRA15% and EuTPI-BPRA20%, G' was lower than G'' at low frequency (Fig. 3-11a), displaying liquid behavior. Moreover, G' and η were drastically reduced at low frequency. Taking EuTPI-BPRA15% for instance, G' was lowered nearly three magnitudes and η was reduced to about 5% compared to those of pure EuTPI at $\omega = 0.1$ rad/s.

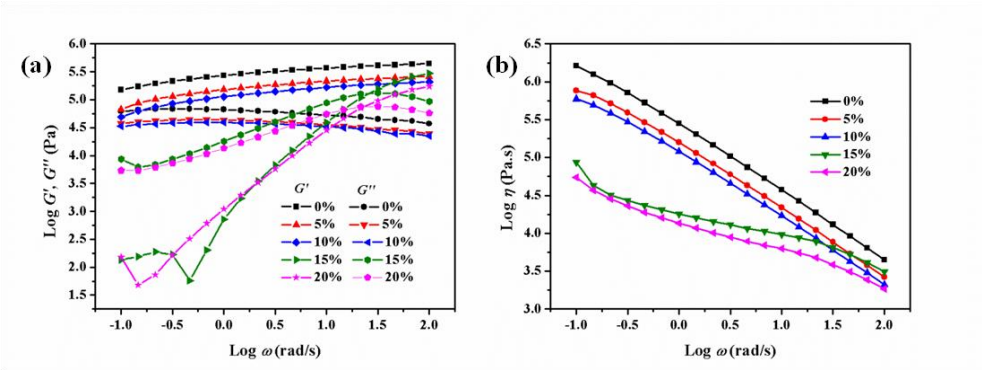

Figure 3-11. Rheological properties of EuTPI, EuTPI-BPRA5%, EuTPI-BPRA10%, EuTPI-BPRA15%, and EuTPI-BPRA20%: (a) frequency-dependent dynamic storage modulus *G'* and loss modulus *G"* curves; (b) frequency-dependent complex viscosity η curves

The mechanical properties of blends of immiscible materials were highly dependent on the morphology, such as the droplet size and the distance between the droplets.[28] When the low content of BPRA was added, the BPRA distributed in the EuTPI matrix in the form of small size of droplets, and the distance between the droplets was long. The mechanical properties of EuTPI matrix were only slightly affected. With the content of BPRA increased, the size of droplets became larger, and the distance between the droplets became shorter, resulting in weakened mechanical strength of EuTPI matrix. The entanglements between the EuTPI chains could be easily released at the low frequency, and the mobility was improved. Moreover, the small

droplets of BPRA functioning as a lubricant to further improve the mobility of EuTPI phase. This also explains the behavior transformation from elastic gel to liquid with the increase of BPRA above melting point of EuTPI. When 20 wt% of BPRA was added, however, the coalescence became serious (Fig. 3-8). Therefore, around 15 wt% of BPRA would be the appropriate value for practical application as the processing aid of EuTPI.

The above results indicate that BPRA was more effective to improve the processing ability of EuTPI compared to LPRA, because BPRA possessed better compatibility with EuTPI, and could exist in the EuTPI matrix as uniform droplets up to the content of 15 wt%.

3.3.4 Thermal properties

The thermal stability of EuTPI, BPRA, and EuTPI-BPRA15% was investigated by TGA. The results (Fig. 3-12) show that both of EuTPI and BPRA possessed good thermal stability.

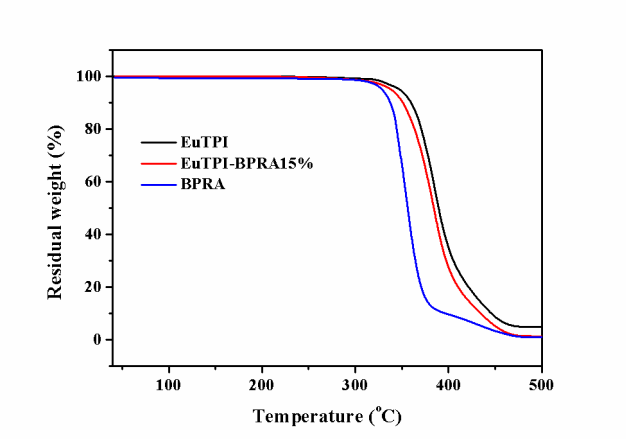

Figure 3-12. TGA curves of BPRA, EuTPI, and EuTPI-BPRA15%.

The decomposition temperature (T_{d5}) of EuTPI and BPRA was 348 °C and 329 °C, respectively. For EuTPI-BPRA15%, T_{d5} was around 338 °C, which indicates the introduction of BPRA would not compromise the thermal stability of EuTPI during the processing and usage.

The crystallization behaviors of EuTPI, EuTPI/LPRA and EuTPI/BPRA blend samples were investigated by DSC. The crystallinity was calculated based on the reported melting enthalpy of 100% pure α-form and β-form crystals of *trans*-1,4-polyisoprene, which are 12.8 KJ/mol and 9.6 KJ/mol repeat unit, respectively.[9] LPRA and BPRA were completely amorphous, because the regular arrangement was disturbed by the dangling chains of polymer. EuTPI showed a crystallization peak at 26 °C during the cooling scan (Fig. 3-13a). Two endothermic peaks locating at 46 °C and 54 °C were observed during the heating process (Fig. 3-13b), which correspond to the transformation from β to α phase and the melting of α phase, respectively.[2,29-31] BPRA and LPRA possessed similar effects on the crystallization of EuTPI (Fig. 3-13 and 3-14). Considering the nonuniform distribution of LPRA in the EuTPI matrix, the influence of BPRA on the crystallization behaviors of EuTPI was mainly discussed. As shown in Table 3-1, crystallinity (χ_c) of EuTPI rapidly decreased from 32 % to 28 % by the addition of 5 wt% of BPRA, then displayed small decrease with the increasing content of BPRA. The blend film still retained high crystallinity (24 %) when 20 wt% of BPRA was introduced. It is believed that BPRA possessed two different effects on the crystallization of EuTPI with respect to the location distribution. Only a small part of BPRA located in the EuTPI phase due to the poor miscibility between BPRA and EuTPI. This part of BPRA functioned as the impurity, disturbing the regular arrangement of EuTPI chains. Most of BPRA existed as

separated droplets. These droplets exerted less influence on the crystallization of EuTPI.

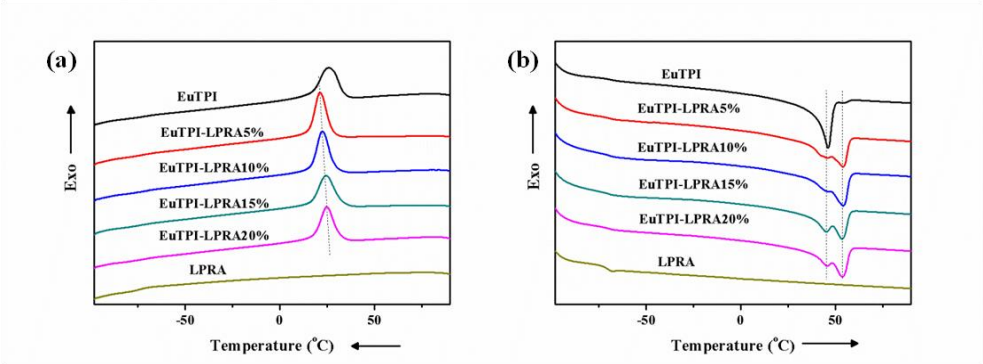

Figure 3-13. DSC traces of LPRA, EuTPI, EuTPI-LPRA5%, EuTPI-LPRA10%, EuTPI-LPRA15%, and EuTPI-LPRA20%: (a) cooling scan; (b) subsequent heating scan.

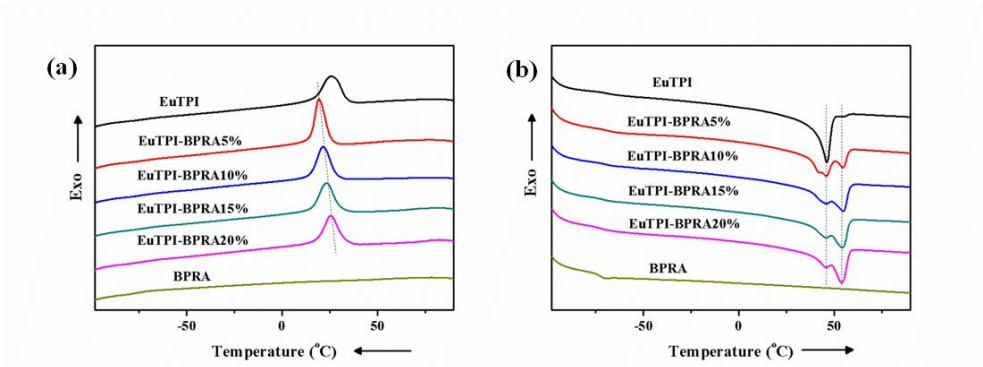

Figure 3-14. DSC traces of BPRA, EuTPI, EuTPI-BPRA5%, EuTPI-BPRA10%, EuTPI-BPRA15%, and EuTPI-BPRA20%: (a) cooling scan; (b) subsequent heating scan.

It is worthy to note that, with increasing the content of BPRA, the ratio of α-phase crystallites first rapidly increased from 2 % to 31 %, finally reached 37 % (Table 3-1). As aforementioned, BPRA existed as two parts: one existed in the EuTPI phase; the other existed as separated droplets. The former part other than the latter part contributed to the increase of α-phase crystallites. Although the former part would suppress the total crystallinity, it could improve the mobility of the EuTPI chains and favor the formation of more stable α-phase crystallites, due to the high mobility, flexibility of BPRA.

Table 3-1. Non-isothermal crystallization of EuTPI and EuTPI-BPRA blend samples

	T_c (°C)	χ_c (%)	α%[a]	β%[b]
EuTPI	26	32	2	98
EuTPI-BPRA5%	20	28	15	85
EuTPI-BPRA10%	22	26	31	69
EuTPI-BPRA15%	23	26	33	67
EuTPI-BPRA20%	26	24	37	63

[a, b] Percentage of the crystallinity of α-phase and β-phase crystallites, respectively.

3.4 Summary

In this chapter, LPRA and BPRA were synthesized using immobilized lipase as catalyst, and both of them were separately introduced into EuTPI to improve the processing ability. BPRA possessed better compatibility with EuTPI compared to LPRA, and could exist in the EuTPI matrix as uniform droplets up to the content of 15 wt%, leading to obvious improvement of processing ability of EuTPI. BPRA also could be chemically incorporated into the crosslinked network of EuTPI through the reaction between C=C bonds of EuTPI and BPRA, which made BPRA difficult to escape from the EuTPI matrix and contributed to the stable performance of the final products. BPRA would serve as a crosslinkable processing aid for EuTPI.

3.5 References

(1) Kent, E. G.; Swinney, F. B. *Ind. Eng. Chem. Prod. Res. Dev.* **1966,** *5*, 134-138.

(2) Goodman, A.; Schilder, H.; Aldrich, W. *Oral. Surg., Oral. Med., Oral. Pathol.* **1974,** *37*, 954-961.

(3) Nakazawa, Y.; Takeda, T.; Suzuki, N.; Hayashi, T.; Harada, Y.; Bamba, T.; Kobayashi, A. *Planta* **2013,** *238*, 549-560.

(4) Tangpakdee, J.; Tanaka, Y.; Shiba, K.; Kawahara, S.; Sakurai, K.; Suzuki, Y. *Phytochemistry* **1997,** *45*, 75-80.

(5) Nakazawa, Y.; Bamba, T.; Takeda, T.; Uefuji, H.; Harada, Y.; Li, X.; Chen, R.; Inoue, S.; Tutumi, M.; Shimizu, T.; Su, Y.; Gyokusen, K.; Fukusaki, E.; Kobayashi, A. *Plant Biotechnol.* **2009,** *26*, 71-79.

(6) Bamba, T.; Fukusaki, E.; Nakazawa, Y.; Kobayashi, A. *Planta* **2002,** *215*, 934-939.

(7) Arvanitoyannis, I.; Kolokuris, I.; Nakayama, A.; Aiba, S. *Carbohydr. Polym.* **1997,** *34*, 291-302.

(8) Tsujimoto, T.; Toshimitsu, K.; Uyama, H.; Takeno, S.; Nakazawa, Y. *Polymer* **2014,** *55*, 6488-6493.

(9) Zhang, J.; Xue, Z. *Polym. Test.* **2011,** *30*, 753-759.

(10) Xue, Z.; Zhang, J.; Li, X.; Yan, R. *International Symposium on Eucommia ulmoides* **2007,** *1*, 116-118.

(11) Yan, R. *International Symposium on Eucommia ulmoides* **2007,** *1*, 34-37.

(12) Sarina; Zhang, J.; Zhang, L. *Polym. Bull.* **2012,** *68*, 2021-2032.

(13) Ogunniyi, D. S. *Bioresour. Technol.* **2006,** *97*, 1086-1091.

(14) Mutlu, H.; Meier, M. A. R. *Eur. J. Lipid Sci. Technol.* **2010,** *112*, 10-30.

(15) Lebarbe, T.; Ibarboure, E.; Gadenne, B.; Alfos, C.; Cramail, H. *Polym. Chem.*

2013, *4*, 3357-3369.

(16) Robertson, M. L.; Paxton, J. M.; Hillmyer, M. A. *ACS Appl. Mater. Inter.* **2011,** *3*, 3402-3410.

(17) Gautrot, J. E.; Zhu, X. X. *Chem. Commun.* **2008,** *0*, 1674-1676.

(18) Ebata, H.; Yasuda, M.; Toshima, K.; Matsumura, S. *J. Oleo Sci.* **2008,** *57*, 315-320.

(19) Ebata, H.; Toshima, K.; Matsumura, S. *Macromol. Biosci.* **2007,** *7*, 798-803.

(20) Shikanov, A.; Domb, A. J. *Biomacromolecules* **2006,** *7*, 288-296.

(21) Kelly, A. R.; Hayes, D. G. *J. Appl. Polym. Sci.* **2006,** *101*, 1646-1656.

(22) Slivniak, R.; Langer, R.; Domb, A. J. *Macromolecules* **2005,** *38*, 5634-5639.

(23) Slivniak, R.; Domb, A. J. *Biomacromolecules* **2005,** *6*, 1679-1688.

(24) Bódalo-Santoyo, A.; Bastida-Rodríguez, J.; Máximo-Martín, M. F.; Montiel-Morte, M. C.; Murcia-Almagro, M. D. *Biochem. Eng. J.* **2005,** *26*, 155-158.

(25) Teomim, D.; Nyska, A.; Domb, A. J. *J. Biomed. Mater. Res.* **1999,** *45*, 258-267.

(26) Krasko, M. Y.; Shikanov, A.; Ezra, A.; Domb, A. J. *J. Polym. Sci., Part A: Polym. Chem.* **2003,** *41*, 1059-1069.

(27) Jannerfeldt, G.; Boogh, L.; Manson, J. A. E. *Polym. Eng. Sci.* **2001,** *41*, 293-300

(28) Chang, K.; Robertson, M. L.; Hillmyer, M. A. *ASC Appl. Mater. Interfaces* **2009,** *1*, 2390-2399.

(29) Anandakumaran, K.; Kuo, C. C.; Mukherji, S.; Woodward, A. E. *J. Polym. Sci.: Polym. Phys. Ed.* **1982,** *20*, 1669-1676.

(30) Cooper, W.; Vaughan, G. *Polymer* **1963,** *4*, 329-340.

(31) Pathak, A.; Saxena, V.; Tandon, P.; Gupta, V. D. *Polymer* **2006,** *47*, 5154-5160.

Chapter 4 Acid-catalyzed synthesis and characterization of hyperbranched poly(ricinoleic acid)

4.1 Introduction

Ricinoleic acid (RA) takes up of approximately 90 % of castor oil, which is low cost and commercially available. RA could form the polyester by the condensation reaction of hydroxyl and carboxylic groups, meanwhile, the unsaturated bonds render RA with cross-linkable properties.[1,2] The antibacterial properties of RA have also been verified by previous reports.[3,4] In recent years, the polyesters from RA have been widely studied.[5-8] It was found that poly(ricinoleic acid) (PRA) with good mechanical properties was difficult to obtain, due to the poor reactivity of RA.[9-11] Although a elastomer was successfully prepared from pure methyl ricinoleate using high loading of lipase as catalyst,[12,13] the high cost of monomer and lipase would inevitably hamper the practical applications. RA as a minor component often copolymerized with other monomers to tune the properties of materials.[3,10,14-19] On the other hand, hyperbranched polymers attract many researchers' attention due to their unique properties such as low viscosity, good film-forming and easy cross-linking properties.[20-22] There were some papers concerning the synthesis of hyperbranched polymers based on castor oil,[8,23,24] in which the content of castor oil was low. A hyperbranched macroinitiator would provide multiple active sites for the polymerization of RA to produce hyperbranched PRA (HBPRA) with high bio-based content. Taking the advantages of hyperbranched structure, the performance of HBPRA would be very interesting for materials science.

In this chapter, HBPRA was synthesized by polycondensation reaction using

polyglycerol (PGL) as the macromolecular initiator and RA as the monomer with *p*-toluenesulfonic acid (PTSA) as catalyst (Fig. 4-1). The reaction conditions, structure, and properties of HBPRA were extensively studied.

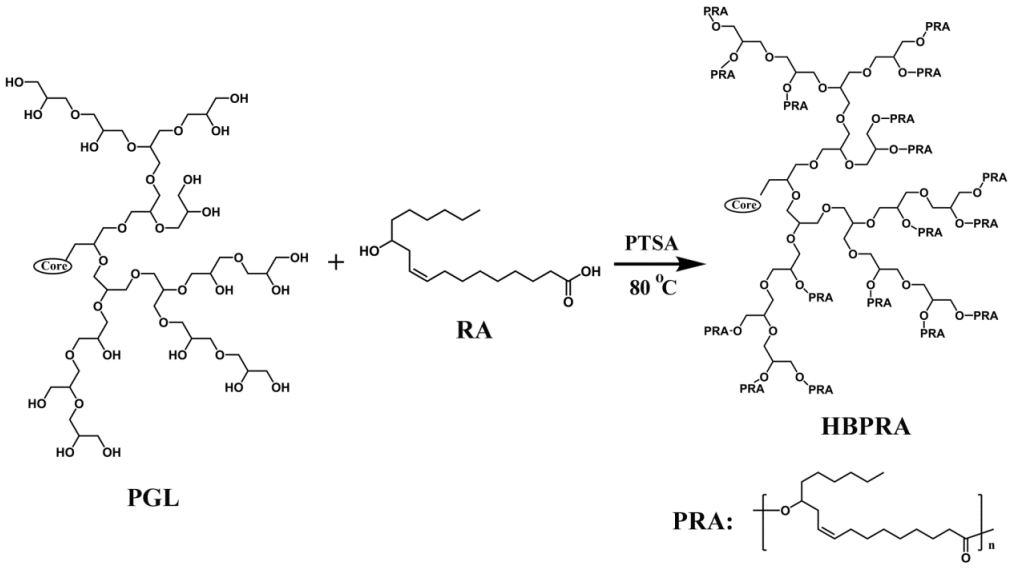

Figure 4-1. Synthetic scheme of HBPRA

4.2 Experimental section

4.2.1 Materials

Ricinoleic acid (RA, > 80 %), trimethylolpropane tris(3-mercaptoproprionate) (TMPMP, > 85 %), and 2,2-dimethoxy-2-phenylacetophenone (DMPA, > 98 %) were purchased from Tokyo Chemical Industry Co, Ltd., Japan. The *p*-toluenesulfonic acid monohydrate (PTSA) was purchased from Wako Pure Chemical Industries, Ltd., Japan. Polyglycerol (PGL, $M_n = 3 \times 10^3$ g/mol, number of hydroxyl groups per molecule = 40) was obtained from Daicel Corporation, Japan. All reagents without special mention were used as received.

4.2.2 Synthesis of PRA

The procedure for the synthesis of PRA was described as follows: RA (20 g, 67 mmol) and PTSA (0.70 g, 3.35 mmol, 5 mol% of RA) were added to a 50 ml of flask with magnetic stirring bar. The flask was heated in 80 °C oil bath and simultaneously evacuated with oil pump for 24 h. Every four hours, the sampling was carried out to monitor the reaction process. After 24 h, the sample was dissolved in 30 ml of THF. The solution was dropped into 300 ml of $NaHCO_3$ (0.56 g) aqueous solution to neutralize the PTSA. The oil layer was collected using separatory funnel and dissolved with 30 ml of THF, followed by reprecipitation in 300 ml of methanol to remove the unreacted monomer and oligomer. The mixture was allowed to stand for overnight at room temperature. Then, the precipitate formed at the bottom layer was collected and dried at 60 °C *in vacuo* for 48 h. The final product was referred to as PRA.

4.2.3 Synthesis of HBPRA

The synthesis of HBPRA was similar to that of PRA. First, PGL (0.5 g, 6.7 mmol of -OH groups), RA (20 g, 67 mmol, 10 times of the number of -OH groups of PGL), and PTSA (0.70 g, 3.7 mmol, 5 mol% of -OH groups of RA and PGL) were added to a 50 ml of flask with magnetic stirring bar, vigorously stirring for 30 min to fully mix the reactants. Afterwards, the flask was heated in 80 °C oil bath and simultaneously evacuated with oil pump for 30 h. At the initial stage, the pressure should be carefully controlled to prevent the eruption of the reactants. After the reaction was quenched by cooling down to room temperature with running water, 30 ml of THF was added to dissolve the crude product, followed by dropping into 300 ml of $NaHCO_3$ (0.62 g) aqueous solution to neutralize the PTSA. The oil layer was collected using

separatory funnel and dissolved with 30 ml of THF, followed by reprecipitation in 300 ml of acetone to remove the unreacted monomer and oligomer. The mixture was allowed to stand for overnight at room temperature. Then, the precipitate formed at the bottom layer was collected and dried at 60 °C *in vacuo* for 48 h. The final transparent liquid product with light yellow color (Fig. 4-2) was obtained and referred to as HBPRA10. According to the same procedure, HBPRA5, HBPRA15, and HBPRA20 were synthesized. As for HBPRA0.5, HBPRA1, and HBPRA3, methanol instead of acetone was used as solvent for the reprecipitation.

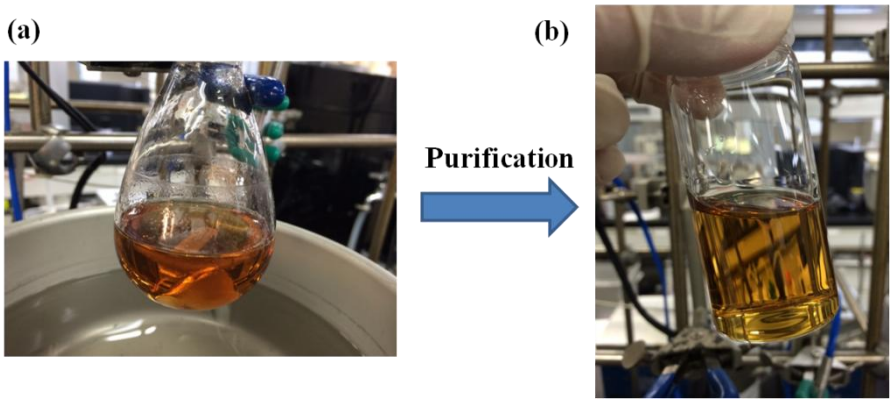

Figure 4-2. Photos of the samples of HBPRA10 (a) after reaction and (b) after purification.

4.2.4 UV-crosslinking of HBPRA10

HPBRA10 (0.5 g), DMPA (5 mg, 1 wt% of HBPRA10), and TMPMP (15 mg, 3 wt% of HBPRA10) were dissolved in 3 ml of $CHCl_3$. The solution was casted on the various substrates (glass plate, Teflon plate, and aluminium foil) and allowed to dry at room temperature for overnight. Then, the sample was exposed to 365 nm of UV light for 30 min. The UV source was a UM-102 high-pressure UV lamp (100 W, from USHIO INC., Japan) equipped with a UV filter centered at 365 nm. The distance between the sample and the light source was set as 10 cm. The sample was postcured in

an air forced oven at 60 °C for 8 h to remove the unreacted TMPMP.

4.2.5 Characterization

Size exclusion chromatography (SEC) analysis was performed on a TOSOH SC-8020 apparatus equipped with refractive index and UV detectors (Tosoh Co., Tokyo, Japan). The column TSKgel G4000H_{XL} was used. The chloroform was used as eluent at a flow rate of 1.0 mL/min at 40 °C. ^{1}H NMR spectra were recorded in $CDCl_3$ using a Bruker DPX-400 instrument (Bruker BioSpin Co., MA, USA). Fourier transform infrared (FT-IR) spectra in the attenuated total reflection (ATR) mode were recorded on a Nicolet iS5 FT-IR spectrometer with iD5 ATR accessory (Thermo Fisher Scientific Inc., Waltham, MA, USA). Thermogravimetric analysis (TGA) was conducted on a SII TG/DTA7200 (Hitachi High-Tech Science Co., Tokyo, Japan) from 40 °C to 500 °C at a heating rate of 10 °C/min under nitrogen. Differential scanning calorimetry (DSC) thermograms were measured using a SII DSC6220 equipment (Hitachi High-Tech Science Co., Tokyo, Japan). The samples were first heated up to 100 °C from room temperature and held for 5 min to eliminate the thermal history, then cooled down to -120 °C and held for 5 min, subsequently heated up from -120 °C to 100 °C at a scanning rate of 10 °C/min under nitrogen. Rheological measurements were performed on a Haake RheoStress 6000 Rheometer (Thermo Fisher Scientific Inc., Waltham, MA, USA) using 20 mm diameter of parallel plates. A stress sweep test was initially performed to ensure that the stress used was within the linear viscoelastic range. Frequency sweeps were executed on each of samples over a frequency range of 0.1~100 rad/s at 25 °C.

4.3 Results and discussion

4.3.1 Structure characterization of PRA and HBPRA

To suppress the side reaction, PRA was polymerized at low reaction temperature (80 °C) using an organic acid catalyst (PTSA). It was found that the reaction took much longer time with the content of PTSA lower than 5 mol%. The reaction time was set as 24 h according to the time courses (Fig. 4-3) of molecular weight and yield of PRA.

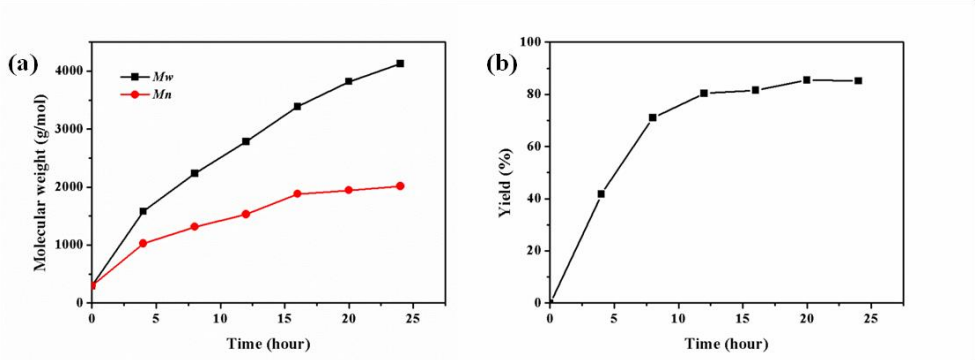

Figure 4-3. Time course of (a) M_w and M_n of PRA and (b) yield of PRA. *The sample was purified by dissolving in small amount of $CHCl_3$ and reprecipitating in 10 ml of methanol.

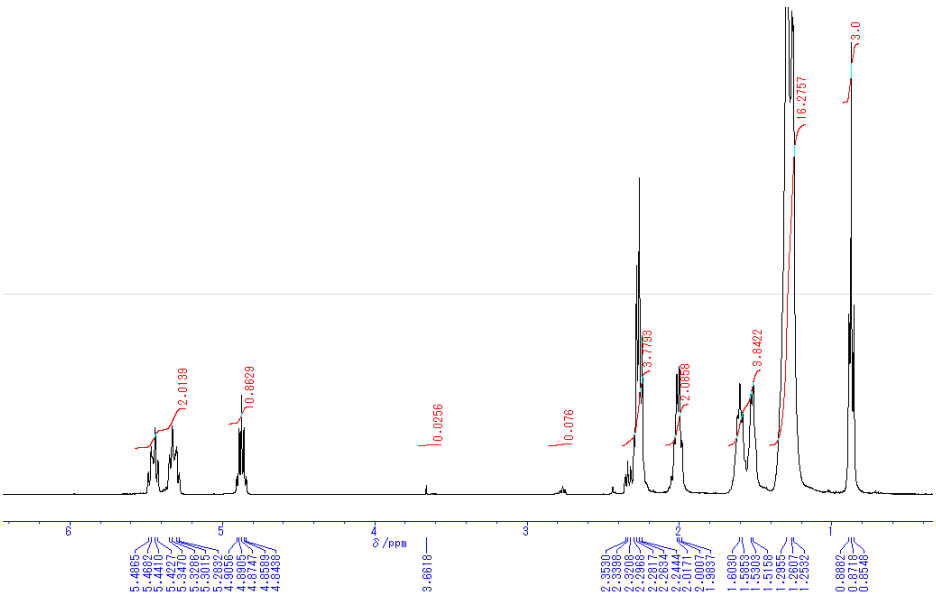

Figure 4-4. ^{1}H NMR spectrum of PRA

The ^{1}H NMR spectrum of PRA (Fig. 4-4) shows that the integrated area ratio (3 : 2) of proton signals belonging to -CH_3 (0.87 ppm) and -CH=CH- (5.2 ~ 5.5 ppm) remains unchanged after the reaction compared to the RA monomer, implying that the -CH=CH- structure remained intact as expected.

PGL was used as the hyperbranched initiator to provide multiple reactive sites for the polymerization of RA. The SEC curves (Fig. 4-5) demonstrate that the samples from HBPRA0.5 to HBPRA15 display a unimodal peak and the peak position gradually shifts toward high-molecular-weight direction, indicating that the molecular weight of HBPRA steadily increased with the increasing ratio of RA to PGL. However, the peak of HBPRA20 almost superposes with HBPRA15 in high molecular weight direction and an obvious shoulder peak appears in low molecular weight direction, suggesting the molecular weight of HBPRA15 already reached the limitation. Above the ratio of 15, self-polymerization would become serious.

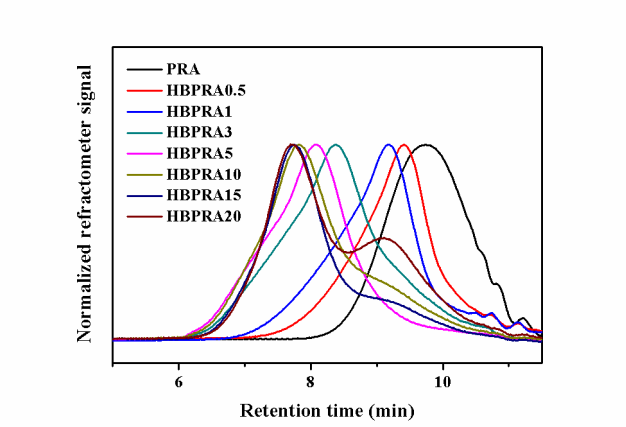

Figure 4-5. SEC curves of PRA, HBPRA0.5, HBPRA1, HBPRA3, HBPRA5, HBPRA10, HBPRA15, and HBPRA20.

Among the HBPRA samples, HBPRA10 was appropriate for further usage due to its high molecular weight and moderate yield (Table 4-1). With respect to the

bio-based PRA component in HBPRA10, PGL was synthesized from petroleum resources. Assuming that all PGL were incorporated into HBPRA10 structure without any loss, the content of PGL in HBPRA10 was calculated to be less than 4 % according to the weight of PGL and the final product, revealing that the bio-based content of HBPRA10 was more than 96 %.

Table 4-1. Properties of PRA and HBPRA

	NMR		GPC			Yield	T_d	T_g
	M_n $\times10^{-3}$	DP*	M_w $\times10^{-3}$	M_n $\times10^{-3}$	PDI	(%)	(°C)	(°C)
PRA	–	–	4.1	2.0	2.1	85	323	-75
HBPRA0.5	–	–	8.8	4.1	2.2	43	314	-63
HBPRA1	–	–	14.1	7.0	2.0	62	298	-64
HBPRA3	52.3	4.4	31.2	9.5	3.3	94	300	-72
HBPRA5	74.8	6.4	44.0	19.5	2.3	80	310	-73
HBPRA10	101	8.7	41.6	11.4	3.6	64	315	-74
HBPRA15	122	10.6	43.1	15.7	2.7	40	319	-74

***** Average degree of polymerization of branch chains of HBPRA.

Although HBPRA10 was not synthesized in a traditional way for the synthesis of hyperbranched polymers, in which small molecules are used as the initiator, and the monomers bear more than two reactive sites to make the chains propagate, the hyperbranched structure with PRA as the dominant component was successfully obtained. Theoretically, HBPRA was composed of a hyperbranched macro-molecular core and 40 branches, and every branch was composed of linear PRA. Since the structure of macro-molecular core would not change, all we need was to characterize the average degree of polymerization (DP) of PRA, which could be easily calculated from

the ^{1}H NMR results (Fig. 4-6), according to the equation DP ≈ [A_f / (A_d + A_a/2) +1]. For HBPRA10, DP of PRA was 8.7. Further, the molecular weight of HBPRA10 was estimated to be 1.0 × 10^5 g/mol according to the following equation:

$$M_{HBPRA} = \{[A_f / (A_d + A_a/2)] +1\} \times (M_{RA}\text{-}M_{water}) \times 40 + M_{PGL}$$

Here, M_{HBPRA}, M_{PGL}, M_{RA}, and M_{water} represent the molecular weight of HBPRA, PGL, RA, and water, respectively. A_a, A_d, and A_f represent the integrated area of the proton signals belonging to H_a, H_d, and H_f of HBPRA, respectively. It is noteworthy that this equation is not suitable for the molecular weight calculation of HBPRA0.5, HBPRA1, and HBPRA20. In the case of HBPRA0.5 and HBPRA1, not all of the hydroxyl groups were reacted. As for HBPRA20, self-polymerization product existed.

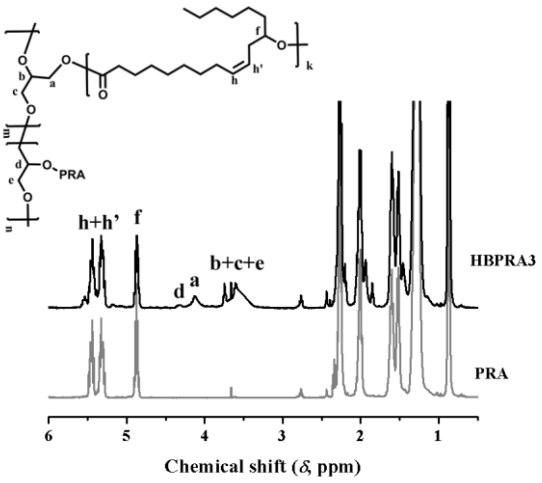

Figure 4-6. ^{1}H NMR spectra of PRA and HBPRA3.

The structure of HBPRA was also studied by FT-IR spectroscopy (Fig. 4-7). With the addition of RA, the peak strength of hydrogen bonds at 3357 cm^{-1} extensively decreases, and the characteristic peak belonging to the stretching mode of carbonyl groups of HBPRA at 1732 cm^{-1} appears. Meanwhile, the position of the characteristic

peak of hydrogen bonds gradually shifts toward high wavenumber, suggesting that the hydrogen bonds became weak with the increasing ratio of RA to PGL. From HBPRA3 to HBPRA20, similar FT-IR spectra were obtained with a very weak peak appearing around 3534 cm^{-1}, implying that the end hydroxyl groups of these samples existed as a free mode rather than hydrogen bonds.

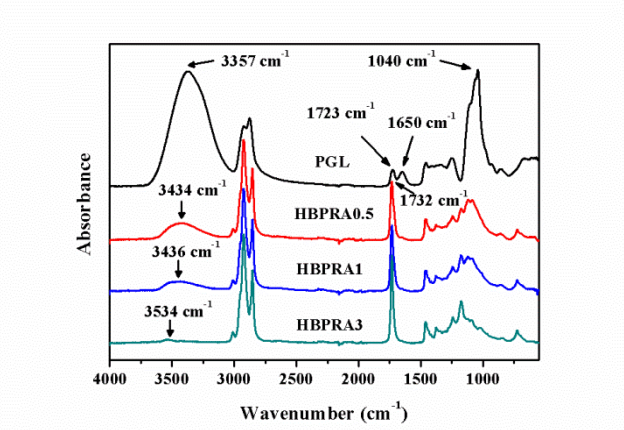

Figure 4-7. FT-IR spectra of PGL, HBPRA0.5, HBPRA1, and HBPRA3

4.3.2 Thermal properties of HBPRA

The thermal stability of HBPRA samples was evaluated by TGA (Fig. 4-8). The thermal decomposition temperature (T_{d10}, the temperature with 10 % of weight loss) of HBPRA samples gradually increases with the increasing ratio of RA to PGL, suggesting that the stability of PRA component of HBPRA was improved with the increasing branch chain length. The DTG results (Fig. 4-8b) show two main peaks from left to right correspond to the thermal decomposition of PRA and PGL component, respectively. The T_{d10} of HBPRA10 was 315 °C (Table 4-1), suggesting its good thermal stability.

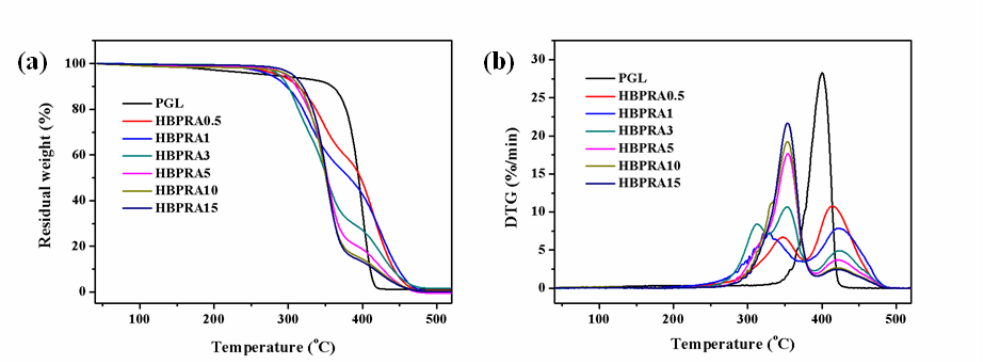

Figure 4-8. (a) TGA curves and (b) DTG curves of PGL, HBPRA0.5, HBPRA1, HBPRA3, HBPRA5, HBPRA10, and HBPRA15.

DSC was also used to study the thermal behaviors of HBPRA samples (Fig. 4-9). With the increasing ratio of RA to PGL, glass transition temperature (T_g) signals of PGL belonging to different generation structure gradually disappear. Instead, the signals of of T_g assigned to PRA component appear, and decrease from the initial -63 °C (HBPRA0.5) to the final -74 °C (HBPRA10). The T_g of HBPRA10 was -74 °C (Table 4-1), which indicates excellent molecular mobility of HBPRA10.

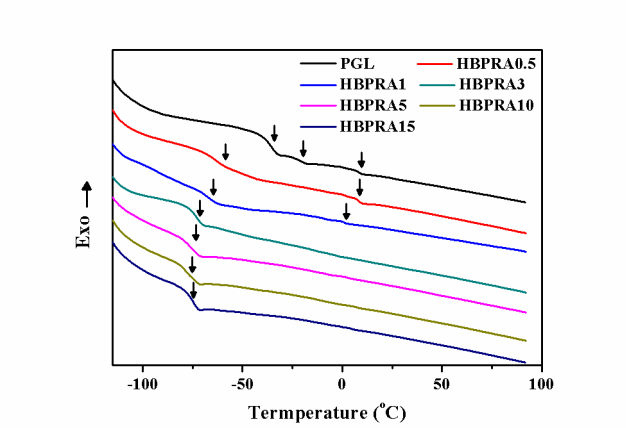

Figure 4-9. DSC curves (the second heating scan) of PGL, HBPRA0.5, HBPRA1, HBPRA3, HBPRA5, HBPRA10, and HBPRA15.

4.3.3 Rheological properties of HBPRA

The rheological properties of HBPRA were systematically investigated. As shown in (Fig. 4-10), the relationship of the complex viscosity (η) versus the frequency (ω) at 25 °C, for all samples from HBPRA0.5 to HBPRA15, displays nearly horizontal lines, suggesting that all HBPRA samples were Newtonian fluid. It was attributed to their hyperbranched structure. Although the molecular weight of HBPRA10 was as high as 1.0×10^5 g/mol, the branch chain length was still not long enough to form entanglements. The η of HBPRA10 at 25 °C was approximately 10 Pa.s. It was believed that the disruption of hydrogen bonds and van der Waals interaction were responsible for the changes of η between different HBPRA samples.

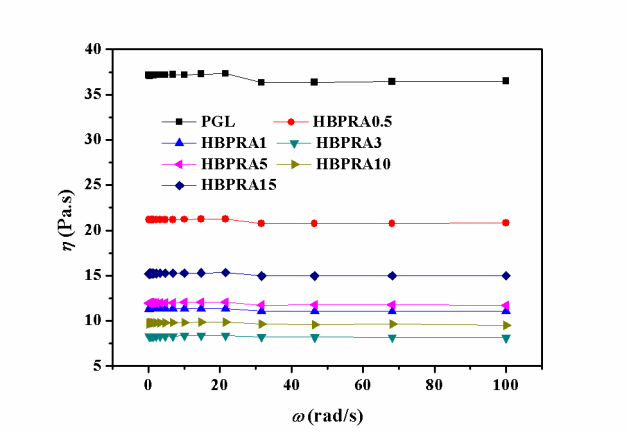

Figure 4-10. Frequency-dependent complex viscosity (η) curves of PGL, HBPRA0.5, HBPRA1, HBPRA3, HBPRA5, HBPRA10, and HBPRA15

4.3.4 Coating film based on HBPRA10

Benefiting from the mild catalyst and low reaction temperature, the double bonds of HBPRA10 were not damaged, and HBPRA10 remained transparent after the reaction. Moreover, by taking advantage of the merits of hyperbranched structure, HBPRA10 possessed good film-forming and easy cross-linking properties. Here, to cure HBPRA10, thio-ene click reaction was used, which is an efficient and robust reaction

system, insensitive to oxygen.[25] HBPRA10 was cross-linked to form a transparent and smooth coating film under UV light for 30 min using catalytic amount of TMPMP (3 wt%) and DMPA (1 wt%). The surface of the coating film was soft but not sticky (pencil hardness ≈ B). Moreover, this coating film well attached to various substrates including glass plate, Teflon plate, and aluminium foil.

4.4 Summary

Based on the above results, it is reasonable to conclude that HBPRA10 was a highly bio-based hyperbranched polymer (PRA component > 96 %), with good thermal stability (T_{d10} = 315 °C), excellent molecular mobility (T_g = -74 °C), low viscosity ($\eta \approx$ 10 Pa.s at 25 °C), good film-forming and easy-crosslinking properties. HBPA10 could be used as promising additive, lubricant, and coating materials.

4.5 References

(1) Mutlu, H.; Meier, M. A. R. *Eur. J. Lipid Sci. Techol.* **2010,** *112*, 10-30.

(2) Ogunniyi, D. S. *Bioresource Technol.* **2006,** *97*, 1086-1091.

(3) Totaro, G.; Paltrinieri, L.; Mazzola, G.; Vannini, M.; Sisti, L.; Gualandi, C.; Ballestrazzi, A.; Valeri, S.; Pollicino, A.; Celli, A.; Di Gioia, D.; Focarete, M. L. *Macromol. Mater. Eng.* **2015**, *300*, 1085-1095.

(4) Vieira, C.; Evangelista, S.; Cirillo, R.; Lippi, A.; Maggi, C. A.; Manzini, S. *Mediat. Inflamm.* **2000,** *9*, 223-228.

(5) Kunduru, K. R.; Basu, A.; Haim Zada, M.; Domb, A. J. *Biomacromolecules* **2015,** *16*, 2572-2587.

(6) Lee, S.; Lee, K.; Kim, Y.; Shin, J. *ACS Sustain. Chem. Eng.* **2015,** *3*, 2309-2320.

(7) Jia, P.; Zhang, M.; Hu, L.; Feng, G.; Bo, C.; Zhou, Y. *ACS Sustain. Chem. Eng.* **2015,** *3*, 2187-2193.

(8) De, B.; Gupta, K.; Mandal, M.; Karak, N. *ACS Sustain. Chem. Eng.* **2014,** *2*, 445-453.

(9) Bódalo-Santoyo, A.; Bastida-Rodríguez, J.; Máximo-Martín, M. F.; Montiel-Morte, M. C.; Murcia-Almagro, M. D. *Biochem. Eng. J.* **2005,** *26*, 155-158.

(10) Slivniak, R.; Langer, R.; Domb, A. J. *Macromolecules* **2005,** *38*, 5634-5639.

(11) Kelly, A. R.; Hayes, D. G. *J. Appl. Polym. Sci.* **2006,** *101*, 1646-1656.

(12) Ebata, H.; Toshima, K.; Matsumura, S. *Macromol. Biosci.* **2007,** *7*, 798-803.

(13) Ebata, H.; Yasuda, M.; Toshima, K.; Matsumura, S. *J. Oleo Sci.* **2008,** *57*, 315-320.

(14) Lebarbe, T.; Ibarboure, E.; Gadenne, B.; Alfos, C.; Cramail, H. *Polym. Chem.* **2013,** *4*, 3357-3369.

(15) Gautrot, J. E.; Zhu, X. X. *Chem. Commun.* **2008,** *0*, 1674-1676.

(16) Teomim, D.; Nyska, A.; Domb, A. J. *J. Biomed. Mater. Res.* **1999,** *45*, 258-267.

(17) Krasko, M. Y.; Shikanov, A.; Ezra, A.; Domb, A. J. *J. Polym. Sci., Part A: Polym. Chem.* **2003,** *41*, 1059-1069.

(18) Shikanov, A.; Domb, A. J. *Biomacromolecules* **2006,** *7*, 288-296.

(19) Havivi, E.; Farber, S.; Domb, A. J. *Polym. Adv. Technol.* **2011,** *22*, 114-118.

(20) Johansson, K.; Bergman, T.; Johansson, M. *ACS Appl. Mater. Interfaces* **2009,** *1*, 211-217.

(21) Gao, C.; Yan, D. *Prog. Polym. Sci.* **2004,** *29*, 183-275.

(22) Yates, C. R.; Hayes, W. *Eur. Polym. J.* **2004,** *40*, 1257-1281.

(23) Bao, Y.; He, J.; Li, Y. *Polym. Int.* **2013,** *62*, 1457-1464.

(24) Güç, E.; Gündüz, G.; Gündüz, U. *Drug Dev. Ind. Pharm.* **2010,** *36*, 1139-1148.

(25) Hoyle, C. E.; Bowman, C. N. *Angew. Chem. Int. Ed.* **2010,** *49*, 1540-1573.

Chapter 5 Biomimic cuticle from hyperbranched poly(ricinoleic acid) and cellulose film

5.1 Introduction

The natural plant cuticle is chiefly composed of two layers. The upper layer is cutin, which is a cross-linked polyester derived from long chain fatty acids. The cutin protects the plant from outer water penetration and pathogen attack. The bottom layer is the polysaccharides, which endow the cuticle with strength and protection from mechanical injury.[1-4] The cuticle structure well balances the advantages of the cutin and polysaccharide, providing the protection for inner plant structure. From the perspective of materials science, the plant cuticle is an ideal bio-based packaging material with well-balanced performance. However, such materials could not be extracted from plants for practical applications. To date, only a few researches were related to the biomimic cutin,[5,6] and the biomimic cuticle has been rarely reported.

For biomimicking cuticle, it is necessary to find suitable hydroxylated fatty acids and polysaccharide resources, which are the main composition of the plant cuticle. Through the thoughtful screening, ricinoleic acid (RA) and cellulose come into my sight. RA [(9Z, 12R)-12-hydroxyoctadec-9-enoic acid] takes up of approximately 90 % of castor oil, which is low cost and commercially available. RA could form the polyester by the condensation reaction of hydroxyl and carboxylic groups, meanwhile, the unsaturated bonds render RA with cross-linkable properties.[7,8] The antibacterial properties of RA have also been verified by previous reports.[9,10] In chapter 4, HBPRA10 was successfully prepared with the content of RA above 96 wt%, which possessed low

viscosity, good film-forming and easy-crosslinking properties, while cellulose is a main kind of polysaccharide, and a transparent cellulose film has been fabricated in chapter 2, theoretically the structure of cuticle could be mimicked based on HBPRA10 and cellulose film (Fig. 5-1).

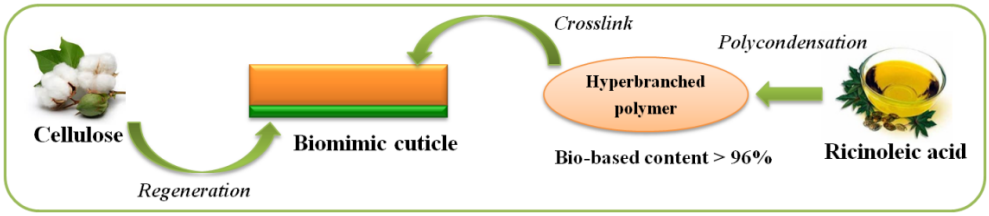

Figure 5-1. Biomimic plant cuticle from RA and cellulose film.

In this chapter, the biomimic cuticle was fabricated from HBPRA10 and cellulose film, with the aid of UV-initiated thio-ene click reaction. The transparency, morphology, surface properties, and mechanical properties of biomimic cuticle were systematically investigated. This study aims to develop a biomimic cuticle with high bio-based content and good performance.

5.2 Experimental section

5.2.1 Materials

Ricinoleic acid (RA, > 80 %), trimethylolpropane tris(3-mercaptoproprionate) (TMPMP, > 85 %), *N*,*N*-dimethylacetamide (DMAc, > 99 %), and 2,2-dimethoxy-2-phenylacetophenone (DMPA, > 98 %) were purchased from Tokyo Chemical Industry Co, Ltd., Japan. Anhydrous lithium chloride (LiCl) and *p*-toluenesulfonic acid monohydrate (PTSA) were purchased from Wako Pure Chemical Industries, Ltd., Japan. Polyglycerol (PGL, M_n = 3 × 10^3 g/mol, number of hydroxyl groups per molecule = 40) was obtained from Daicel Corporation, Japan. Whatman

CF11 fibrous medium cellulose powder (CF11, cotton origin, 50-350 μm, GE Healthcare Life Science Corp., Piscataway, NJ, USA) was used as cellulose resource. All reagents without special mention were used as received.

5.2.2 Fabrication of biomimetic plant cuticle

Cellulose film with the thickness around 20 μm was fabricated according to the method described in chapter 2. The obtained cellulose film was fixed on a glass plate with adhesive tape (Fig. 5-2). HPBRA10 (0.5 g), DMPA (5 mg, 1 wt% of HBPRA10), and TMPMP (15 mg, 3 wt% of HBPRA10) were dissolved in 3 ml of $CHCl_3$. The solution was casted on the cellulose film and allowed to dry at room temperature for overnight. Then, the sample was exposed to 365 nm of UV light for 30 min. The UV source was a UM-102 high-pressure UV lamp (100 W, from USHIO INC., Japan) equipped with a UV filter centered at 365 nm. The distance between the sample and the light source was set as 10 cm. The sample was postcured in an air forced oven at 60 °C for 8 h to remove the unreacted TMPMP. The thickness of sample was around 120 μm; therefore the sample was referred to as biomimic cuticle-120. Through changing the concentration of HBPRA, a sample with thickness about 60 μm was obtained and referred to as biomimic cuticle-60.

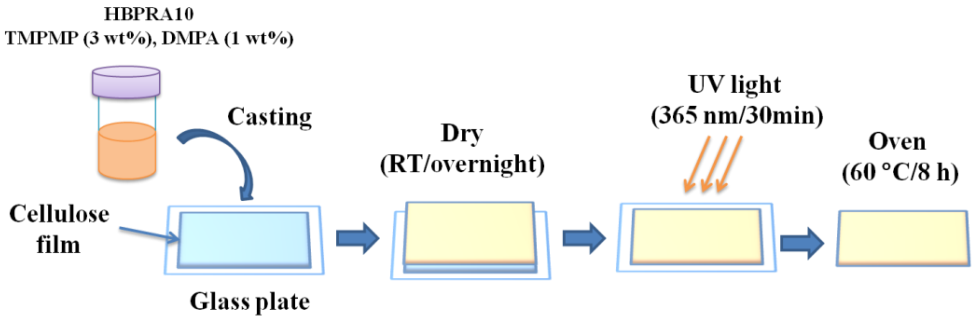

Figure 5-2. Procedure of the biomimic cuticle fabrication.

5.2.3 Characterization

Fourier transform infrared (FT-IR) spectra in the attenuated total reflection (ATR) mode were recorded on a Nicolet iS5 FT-IR spectrometer with iD5 ATR accessory (Thermo Fisher Scientific Inc., Waltham, MA, USA). The optical transmittances of the films were measured from 200 to 900 nm using a Hitachi U2810 UV-visible spectrophotometer. Contact angles (CA) were measured with a Drop Master DM300 instrument (Kyowa Interface Science Co. Ltd, Saitama, Japan) using FAMAS Basic software. Scanning electron microscopic (SEM) analysis was carried out by a Hitachi SU-3500 instrument (Hitachi High-Technologies Co., Tokyo, Japan). Tensile properties were measured by a Shimadzu EZ Graph instrument equipped with a 500 N load cell (Shimadzu Corp., Kyoto, Japan). A crosshead speed of 1 mm/min was used. The sample was cut into rectangular strips 40 mm × 5 mm and tested with a span length of 10 mm. Seven samples were tested and at least 5 samples were chosen.

5.3 Results and discussion

5.3.1 Fabrication of biomimic cuticle

In chapter 4, a transparent and smooth coating film was prepared from HBPRA10 through UV-initiated thio-ene click reaction, and the surface of the coating film was soft but not sticky. However, one problem frustrated me, which was that the intact film could not be peeled off from the substrates including Teflon plate, glass plate, and aluminium foil, due to the strong binding force of the HBPRA film to substrates. This is beneficial for usage in the coating or adhesive area. Nevertheless, it is not the final goal.

Instead of trying to obtain an intact HBPRA10 film to combine the cellulose for fabricating biomimic cuticle, we directly cured the HBPRA on the surface of cellulose film (Fig. 5-2). A highly transparent cellulose film was prepared according to our previous report,[35] and fixed on the glass plate with adhesive tape. This cellulose film was used as a minor component, functioning as a substrate. Then, the $CHCl_3$ solution containing HBPRA10, TMPMP, and DMPA was casted on the cellulose film surface. With the aid of UV-initiated thio-ene click reaction, HBPRA was cross-linked, and a highly transparent biomimic cuticle was obtained (Fig. 5-3). Through altering the concentration of HBPRA10 solution, the thickness of biomimic cuticle could be tuned. In this study, the biomimic cuticles with two different thickness were prepared, which were biomimic cuticle-120 and biomimic cuticle-60. Since the thickness of original cellulose film was around 20 μm, the thickness of HBPRA10 layer was estimated to be 100 μm and 40 μm, respectively. The cellulose layer and HBPRA10 layer could not be differentiated any more by naked eyes due to the high transparency of biomimic cuticle.

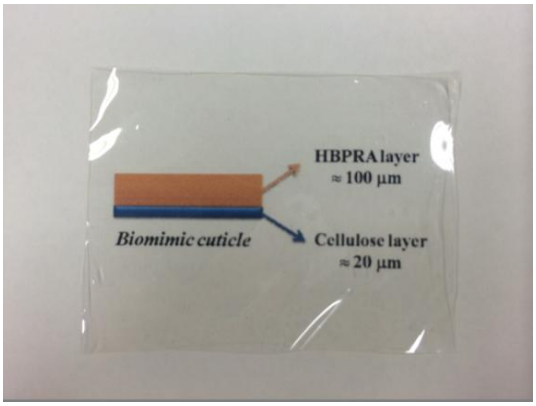

Figure 5-3. Photo of biomimic cuticle-120.

5.3.2 Transparency of biomimic cuticle

The transparency of biomimic cuticle was studied by UV-visible spectroscopy.

Fig. 5-4 shows that the transmittance of biomimic cuticle-60 and biomimic cuticle-120 is comparable (about 90 %) in the visible light range, and the transmittance of the former is only a little higher than that of the latter in the ultraviolet light range, which indicates that both of biomimic cuticle samples possessed high transparency that was less affected by the thickness of samples. Compared to cellulose film, the ultraviolet light was effectively blocked, suggesting that the biomimic cuticle could minimize the damage of UV light.

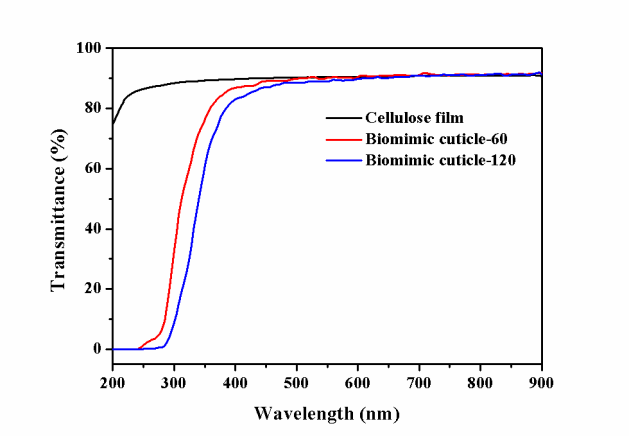

Figure 5-4. Transmittance of cellulose film, biomimic cuticle-60, and biomimic cuticle-120 in the UV-visible wavelength.

5.3.3 Micromorphology of biomimic cuticle

The micromorphology was investigated by SEM. Both of the cellulose side and HBPRA10 side of biomimic cuticle displayed smooth surfaces (Fig. 5-5). No obvious difference was observed. The cross sections of the biomimic cuticle clearly demonstrated double-layer structure (Fig. 5-6), corresponding to the cellulose and HBPRA10 component, which were confirmed by FI-IR spectra (Fig. 5-7). The two layers were perfectly attached, and no gap or crack existed. Moreover, the thickness of the two layers based on the scale bar well matched the previous estimation.

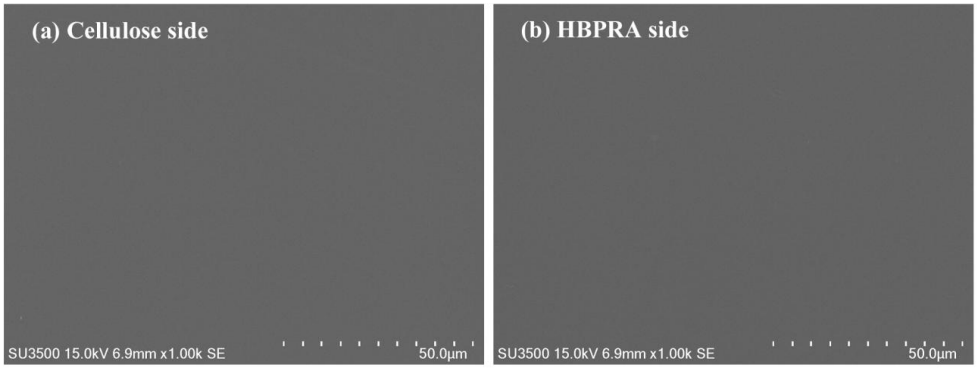

Figure 5-5. SEM images of the biomimic cuticle surfaces of (a) cellulose side and (b) HBPRA side.

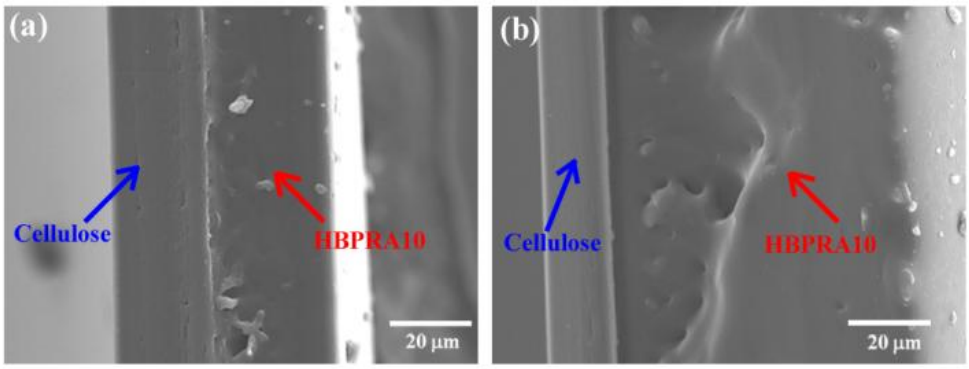

Figure 5-6. SEM images of cross sections of (a) biomimic cuticle-60 and (b) biomimic cuticle-120.

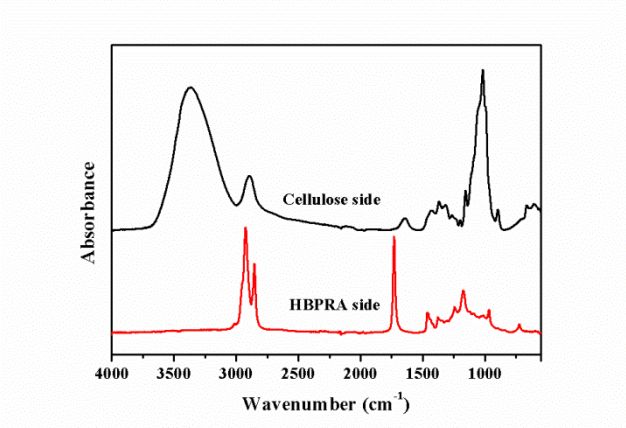

Figure 5-7. FT-IR spectra of the biomimic cuticle surfaces.

The strong binding force to the substrates was an obstacle for us to get an intact film of HBPRA10, but here it contributed to the perfect attachment of the cellulose layer and HBPRA10 layer. Meanwhile, the perfect attachment together with dense

structure of the cellulose layer and HBPRA10 layer contributed to the excellent transparency of biomimic cuticle.

5.3.4 Surface properties of biomimic cuticle

The two surfaces of biomimic cuticle displayed significant differences. The cellulose side possessed hard and slippery surface (pencil hardness > 6H), whereas the HBPRA10 side was soft but not sticky (pencil hardness ≈ B), and could attach to various substrates under gentle force, such as glass and metal. The biomimic cuticle could be used as a promising displaying material with the HBPRA10 side attached to the displaying screen and the cellulose side toward outside (Fig. 5-8).

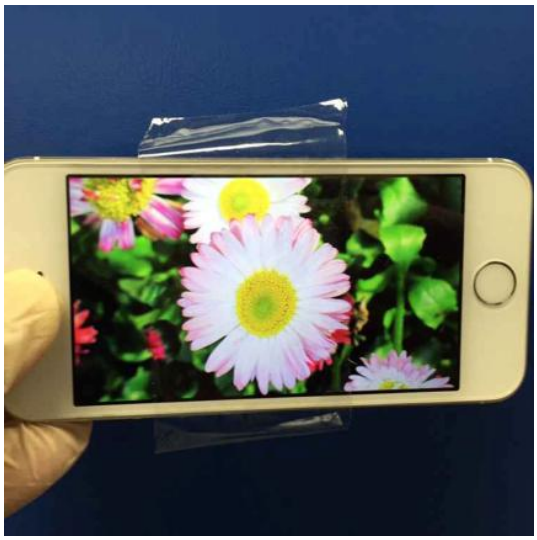

Figure 5-8. Photo of biomimic cuticle attached to the displaying screen of cell phone.

In addition, the two surfaces of biomimic cuticle showed different CA of water, which were 44° and 91° (Fig. 5-9) corresponding to the cellulose side and HBPRA10 side, respectively. This indicates that the cellulose side of biomimic cuticle was hydrophilic and the HBPRA10 side was hydrophobic. Such a structure is beneficial to

applications for packaging materials. For example, when biomimic cuticle is used as a packaging material of fruits, the HBPRA10 layer used as outer layer could prevent outer water and pathogen invasion, and the cellulose layer used as inner layer is helpful to provide strength and retain water from the fruits, just as the plant cuticle does. So, one can choose different side of biomimic cuticle as outer layer depending on the applications.

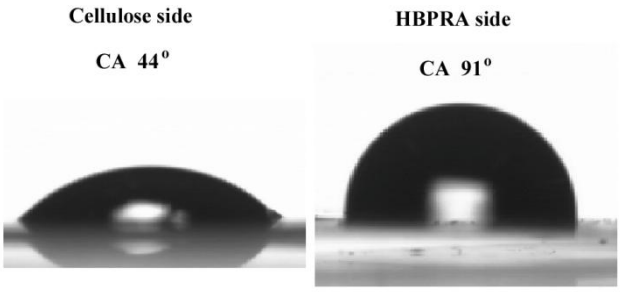

Figure 5-9. Contact angle images of biomimic cuticle-120 surfaces of (a) cellulose side and (b) HBPRA side.

5.3.5 Tensile properties of biomimic cuticle

The mechanical properties of the biomimic cuticle were evaluated by tensile test (Fig. 5-10). The smooth tensile curves suggest that cellulose layer and HBPRA10 layer remained the combining state during stretching process and no slide phenomenon occurred in the interface, which was attributed to the excellent adhesive abilities of HBPRA10. On the other hand, it was extremely difficult to quantitively analyze the interface interactions of the two layers due to the strong attachment. The biomimic cuticle behaved as a tough plastic material. The elongation at break and maximum stress of biomimic cuticle-60 were 39 % ± 3 % and 53 ± 2 MPa, respectively. Those of biomimic cuticle-120 were 44 % ± 2 % and 29 ± 1 MPa, respectively. With the HBPRA10 layer got thicker, the maximum stress of biomimic cuticle obviously

decreased, while only a slight increase was displayed for the elongation at break, suggesting that the mechanical properties of biomimic cuticles largely depended on cellulose film. Compared to the cellulose film (24%, 157 MPa), the maximum stress of bimimic cuticle-120 was lower, but the elongation at break was improved. It is worth noting that cellulose film was only used as a minor component in the biomimic cuticle. Additionally, compared to the major component of HBPRA10, the mechanical properties became much better, since we even cannot obtain the intact HBPRA10 film.

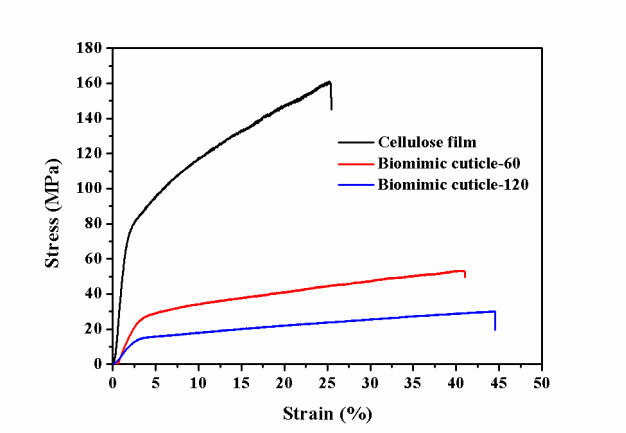

Figure 5-10. Stress-strain curves of cellulose film, biomimic cuticle-60 and biomimic cuticle-120.

5.4 Summary

The biomimic plant cuticle was successfully fabricated from HBPRA10 (bio-based content > 96%) and cellulose film through UV-initiated thio-ene click reaction. Cellulose layer provided the composite film with mechanical strength, while HBPRA layer protected the composite film from water invasion and possessed potential anti-bacterial properties.[9,10] The biomimic cuticle had high transmittance in the visible light region, and the ultraviolet light with the wavelength between 200 ~ 300 nm was effectively blocked to minimize the damage caused by ultraviolet light. To the best of

our knowledge, it is the first time that a double-layer composite film having similar composition and functions with plant cuticle has been obtained. The biomimic cuticle would have potential applications for packaging and displaying materials.

5.5 References

(1) Nawrath, C. *Curr. Opin. Plant Biol.* **2006,** *9,* 281-287.

(2) Dominguez, E.; Cuartero, J.; Heredia, A. *Plant Sci.* **2011,** *181,* 77-84.

(3) Pollard, M.; Beisson, F.; Li, Y. H.; Ohlrogge, J. B. *Trends Plant Sci.* **2008,** *13,* 236-246.

(4) Dominguez, E.; Heredia-Guerrero, J. A.; Heredia, A. *New Phytol.* **2011,** *189,* 938-949.

(5) San-Miguel, M. A.; Oviedo, J.; Heredia-Guerrero, J. A.; Heredia, A.; Benitez, J. J. *J. Mol. Model.* **2014,** *20,* 1-7.

(6) Heredia-Guerrero, J. A.; Heredia, A.; Garcia-Segura, R.; Benitez, J. J. *Polymer* **2009,** *50,* 5633-5637.

(7) Mutlu, H.; Meier, M. A. R. *Eur. J. Lipid Sci. Tech.* **2010,** *112,* 10-30.

(8) Ogunniyi, D. S. *Bioresource Technol.* **2006,** *97,* 1086-1091.

(9) Totaro, G.; Paltrinieri, L.; Mazzola, G.; Vannini, M.; Sisti, L.; Gualandi, C.; Ballestrazzi, A.; Valeri, S.; Pollicino, A.; Celli, A.; Di Gioia, D.; Focarete, M. L. *Macromol. Mater. Eng.* **2015**, *300,* 1085-1095.

(10) Vieira, C.; Evangelista, S.; Cirillo, R.; Lippi, A.; Maggi, C. A.; Manzini, S. *Mediat. Inflamm.* **2000,** *9,* 223-228.

Chapter 6 Concluding remarks

The main topics of this thesis were related to the bio-base materials prepared from ricinoleic acid (RA) and cellulose (Fig. 6-1).

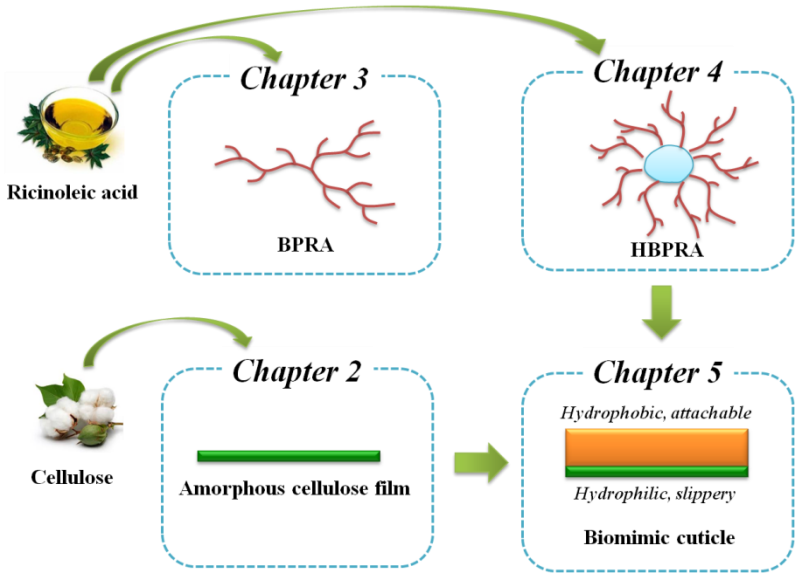

Figure 6-1. Flow of main work of this thesis

In chapter 2, a highly transparent cellulose film (ACF) was prepared from cellulose solution in LiCl/DMAc by regeneration with acetone. The obtained ACF possessed dense, smooth surface, and excellent transparency. The X-ray diffraction results indicated that ACF was highly amorphous, which was further confirmed by solid-state ^{13}C-NMR and FT-IR spectra. Tensile analysis implied that the elongation at break (23.9%) and maximum stress (157 MPa) of ACF that derived from Whatman CF11 fibrous cellulose were higher than those of cellophane (19.9% and 135 MPa, respectively). In addition, enzymatic hydrolysis of ACF and cellophane showed higher hydrolysis rate of the former (about 7 times higher than the latter), indicating

outstanding environmental friendliness. This work provided a simple, less-destructive, and universal method to prepare transparent ACF, which may serve as a promising packaging material to replace cellophane.

In chapter 3, a tri-branched poly(ricinoleic acid) (BPRA) was successfully synthesized using castor oil as the initiator and ricinoleic acid as the monomer with the lipase PS as the catalyst. For comparison, linear poly(ricinoleic acid) (LPRA) was also synthesized using similar method. An interesting application of BPRA was demonstrated, as a processing aid to effectively improve the processing ability of natural *trans*-1,4-polyisoprene extracted from *Eucommia ulmoides* Oliver (EuTPI). SEM observation suggested that BPRA was uniformly distributed in the EuTPI matrix in contrast to the poor distribution of LPRA, and BPRA was effectively incorporated into the crosslinked network of EuTPI by curing with dicumyl peroxide. Rheological studies indicated that BPRA was more effective to improve the processing ability of EuTPI than LPRA. The storage modulus, loss modulus, and complex viscosity (η) of EuTPI over the frequency (ω) range from 0.1 to 100 rad/s at 80 °C obviously decreased with the increasing content of BPRA. At low frequency, the rheological behavior of EuTPI changed from elastic gel to liquid when 15 wt% of BPRA was added. Moreover, η dramatically decreased to about 5% of that of the pure EuTPI at ω = 0.1 rad/s. TGA results suggested that the blending of BPRA would not compromise the thermal stability of EuTPI. BPRA was found to promote the formation of more stable α-phase crystallites of EuTPI by DSC analysis.

In chapter 4, a hyperbranched poly(ricinoleic acid) (HBPRA) was prepared using PGL as the macro-molecular initiator and ricinoleic acid as the monomer with *p*-toulenesulfonic acid as the catalyst. HBPRA as a highly bio-based hyperbranched

polymer (biobased content > 96 wt%) may have promising applications for lubricant, additive, adhesive, and coating materials due to its good thermal stability (T_{d10} = 315 °C), low T_g (-74 °C) and viscosity ($\eta \approx 10$ Pa.s at 25 °C), easy cross-linking and good film-forming properties.

In chapter 5, the biomimic plant cuticle was successfully fabricated from HBPRA and cellulose film with the aid of UV-initiated thio-ene click reaction. This biomimic cuticle possessed excellent transparency (transmittance ≈ 90 % in the visible light range). The SEM observation showed that the biomimic cuticle was composed of two layers, which were perfectly attached. The properties of two surfaces of biomimic cuticle displayed significant differences. Cellulose side was hydrophilic with contact angle (CA) around 44° and pencil hardness > 6H. On the contrary, HBPRA side was hydrophobic with CA about 91° and pencil hardness ≈ B. With respect to the slippery cellulose side, HBPRA side could attach to various substrates under gentle force. In addition, the tensile test showed good mechanical properties. The elongation at break and maximum stress of biomimic cuticle were 44 % and 29 MPa, respectively. The above results suggest that the biomimic cuticle may have potential applications for packaging and displaying materials.

The main achievements of this doctoral thesis list as follows: (1) the successful fabrication of ACF, which will be helpful for understanding the relationship between the structure and properties of cellulose; (2) the synthesis of a hyperbranched macromolecule composed of nearly hundred percent of RA, which shows the possibility that high performance materials could be prepared from low-cost biobased fatty acid, and encourages the wide applications of fatty acid in near future; (3) the design and realization of a double-layer composite film, which well balances the advantages of

ACF and HBPRA, and provides a alternative way for the fabrication of the composite film. The whole thesis surrounds the preparation and applications of biobased and biodegradable materials, and will contribute to the sustainable development of the human society.

List of publications

1. Preparation and characterization of a transparent amorphous cellulose film

   Bo-xing Zhang**,** Jun-ichi Azuma, Hiroshi Uyama*

   RSC Advances **2015,** *5*, 2900-2907.

2. Improvement of rheological properties of *trans*-1,4-polyisoprene from *Eucommia ulmoides* Oliver by tri-branched poly(ricinoleic acid)

   Bo-xing Zhang, Jun-ichi Azuma, Shinya Takeno, Nobuaki Suzuki, Yoshihisa Nakazawa, Hiroshi Uyama*

   Polymer Journal, accepted.

3. Biomimic plant cuticle from hyperbranched poly(ricinoleic acid) and cellulose film

   Bo-xing Zhang, Hiroshi Uyama*

   ASC Sustainable Chemistry & Engineering **2016**, *4*, 363-369.

Acknowledgements

This study was carried out from 2013 to 2016 at the Department of Applied Chemistry, Graduate School of Engineering, Osaka University.

First and foremost, I would like to express my deepest gratitude to my supervisor Prof. Hiroshi Uyama, Department of Applied Chemistry, Graduate School of Engineering, Osaka University, for providing me with the chance to study at Osaka University as a PhD student three year ago. I also want to thank him for the invaluable help and guidance during my study.

I want to give special thanks to Prof. Jun-ichi Azuma, who has been giving me a lot of help and guidance since the beginning of this study. I learn much knowledge about cellulose and plant cuticle from him, also his enthusiasm to the scientific research deeply impresses me.

I would like to express my sincere appreciation to Assistant Prof. Takashi Tsujimoto for his kind help all this time. Without his help, this thesis could not be smoothly done.

I am especially grateful to Assistant Prof. Urara Hasegawa and Dr. André J. van der Vlies for their kind help and suggestions.

I would like to express great thanks to Prof. Hidehiro Sakurai and Prof. Satoshi Minakata for their constructive comments and precious time on reviewing this thesis.

I also appreciate the help from Prof. Susumu Kuwabata and Assistant Prof. Taro Uematsu for the TEM measurement, and Prof. Nobuhito Imanaka and Associated Prof. Shinji Tamura for the XRD measurement.

I am very thankful to the present and past members of Uyama Lab, Ms. Yoko

Uenishi, Ms. Tomoko Shimizu, Dr. Yasushi Takeuchi, Dr. Yuanrong Xin, Dr. Xiaoxia Sun, Dr. Wenjuan Han, Dr. Nao Hosoda, Dr. Masaki Moriyama, Dr. Guowei Wang, Ms. Hitomi Fukuda, Mr. Naoya Tateishi, Mr. Ken-ichi Toshimitsu, Mr. Tengjiao Wang, Ms. Hyunhee Shim, Ms. Ayumi Dobashi, Ms. Manami Morisaki, Mr. Tomoki Kasahara, Ms. Yu Shu, Mr. Zhibin Huang, Mr. Qidong Wang, Mr. Tomonari Kanno, Mr. Keng Yao Tan, Ms. Jingyuan Niu, Ms. Xingyu Xiang, Mr. Jia Yu Chen, Ms. Hoi I Neng, etc. for their kind help and cooperation.

Financial support from China Scholarship Council (CSC) is also acknowledged.

Finally, I would like to thank my family for their always understanding and supporting. The love and encouragement from them are the resource of power that keeps me moving forward.

January, 2016
Bo-xing Zhang